Delft University of Technology

A general substructure-based framework for input-state estimation using limited output measurements

Tatsis, K. E.; Dertimanis, V. K.; Papadimitriou, C.; Lourens, E.; Chatzi, E. N.

Important note
To cite this publication, please use the final published version (if applicable).
Please check the document version above.

A general substructure-based framework for input-state estimation using limited output measurements

K.E. Tatsis [a],[*], V.K. Dertimanis [a], C. Papadimitriou [b], E. Lourens [c], E.N. Chatzi [a]

[a] *Institute of Structural Engineering, Department of Civil, Environmental and Geomatic Engineering, ETH Zürich, Stefano-Franscini-Platz 5, 8093 Zürich, Switzerland*
[b] *Department of Mechanical Engineering, University of Thessaly, Leoforos Athinon, Pedion Areos, 38334 Volos, Greece*
[c] *Faculty of Civil Engineering and GeoSciences, Delft University of Technology, Stevinweg 1, 2628 CN Delft, The Netherlands*

ABSTRACT

This paper presents a general framework for estimating the state and unknown inputs at the level of a system subdomain using a limited number of output measurements, enabling thus the component-based vibration monitoring or control and providing a novel approach to model updating and hybrid testing applications. Under the premise that the system subdomain dynamics are driven by the unknown (i) externally applied inputs and (ii) interface forces, with the latter representing the unmodeled system components, the problem of output-only response prediction at the substructure level can be tailored to a Bayesian input-state estimation context. As such, the solution is recursively obtained by fusing a Reduced Order Model (ROM) of the structural subdomain of interest with the available response measurements via a Bayesian filter. The proposed framework is without loss of generality established on the basis of fixed- and free-interface domain decomposition methods and verified by means of three simulated Wind Turbine (WT) structure applications of increasing complexity. The performance is assessed in terms of the achieved accuracy on the estimated unknown quantities.

© 2020 The Author(s). Published by Elsevier Ltd. This is an open access article under the CC BY-NC-ND license (http://creativecommons.org/licenses/by-nc-nd/4.0/).

1. Introduction

The problem of model-based response prediction on the basis of a limited number of vibration measurements has received significant attention in recent years. Within this context, research has been oriented towards methodologies for input reconstruction [1–3], with the aim of relaxing the requirement for excitation measurements, while considerable emphasis has been also placed on recursive methodologies for online applications [4,5]. As such, a number of Bayesian algorithms [6–9] for the joint estimation of states, unknown input and/or parameters [10] of linear and non-linear systems has been to date well established, and validated [11]. Although the predictions of such estimators are naturally suited for structural control implementations [12], they can be alternatively exploited for numerous objectives, such as system identification [13,14], damage detection [15,16] and fatigue assessment [17–20] among others.

Despite their efficient performance in terms of the estimated state, input and parameters, the existing inverse methodologies for state estimation with unknown inputs have been so far formulated and applied in the full system domain, which implies that their implementation requires modeling information of the entire system. The latter is oftentimes a limiting factor for actual engineering applications, since the various noise sources existing at the system level are not straightforwardly quantifiable through the filter covariance matrices. Bridges are typical civil structures of such applications, where significant

---

model errors are inevitably introduced from the unknown loads due to wind, as well as from the unaccounted for traffic-induced vibrations. Similarly, the model-based prediction of the dynamic state of Wind Turbines (WTs) in a global framework becomes a challenging and computationally prohibitive task. This is due to the inherently stochastic nature of WTs, which originates from a number of uncertain environmental, operational and structural factors that are to a large extent related to the aerodynamics. To overcome this hurdle, a subdomain inverse approach would be required [21–25], which would thus circumvent the requirement for modeling intricate and time-varying dynamics and would further reduce the level of modeling errors and allow for optimal estimation.

In this contribution, a general component-based Bayesian framework for output-only response prediction of systems with limited sensing points is proposed. The methodology is based on the decomposition of a system into substructures that can be treated and modeled independently of the entire system. As such, the response prediction at the level of a subsystem can be viewed as an input-state estimation problem with the interface forces acting as unknown inputs on top of the probably existing external loads. Apart from the fact that a subdomain-based solution to the problem of dynamic state estimation is thereby enabled, the proposed methodology features a number of additional benefits that can be exploited for various engineering applications. Namely, the assumptions associated with the spatial distribution of the unknown, and oftentimes equivalent [26], inputs can be avoided, especially when dealing with components whose dynamics are solely driven by the interface forces. With model uncertainty constituting one of the major issues related to the tuning of Kalman-type filters, a component-based approach leads to considerably reduced modeling errors which in turn facilitate the tuning process. The methodology is further well suited for component-based model updating [27] as well as for hybrid-testing applications [28] and limited-resource monitoring projects [29], where instrumentation of the entire system is not feasible.

The structure of this paper is organized as follows: the general framework for dynamic substructuring using either fixed- or free-interface approaches is presented in Section 2, along with the reduction ingredients of each method, including interface and rigid body modes. The integration of substructure models into the context of input and state estimation on the basis of limited vibration response measurements is documented in Section 3. Lastly, Section 4 presents a set of case studies illustrating the performance and outlining the specifics of the proposed framework for different engineering problems, while the conclusions are summarized in Section 5.

2. Substructuring formulation

This section provides the necessary background for substructure reduced-order modeling, whereon the proposed framework for vibration-based response prediction using limited output measurements is based. In view of the extensive literature on substructuring, this section aims at comprehensively presenting the different substructure ingredients required for establishing the proposed framework and further introducing the notation to be used in the following section for Bayesian filtering. In so doing, a linear Finite Element (FE) model, defined on a domain Ω, is initially considered, whose continuous-time dynamics are described by the second-order differential equations

$$\mathbf{M}\ddot{\mathbf{u}}(t) + \mathbf{C}\dot{\mathbf{u}}(t) + \mathbf{K}\mathbf{u}(t) = \mathbf{f}(t) \tag{1}$$

with initial conditions $\mathbf{u}(0) = \mathbf{u}_0$ and $\dot{\mathbf{u}}(0) = \dot{\mathbf{u}}_0$, where $\mathbf{u}(t) \in \mathbb{R}^n$ is the displacement vector, $\mathbf{M}, \mathbf{C}, \mathbf{K} \in \mathbb{R}^{n \times n}$ are the mass, damping and stiffness matrices and $\mathbf{f}(t) \in \mathbb{R}^n$ is the excitation vector.

The FE domain Ω described by Eq. (1) may be further divided into a number of non-overlapping subdomains $\Omega^{(s)}$, for $s = 1, 2, \ldots, N_s$, so that each node of the FE model belongs to exactly one substructure, except for those lying on the interfaces. Upon omitting the explicit time-dependency, the dynamic response of the N_s uncoupled substructures may be described by the block-diagonal system of equations

$$\begin{bmatrix} \mathbf{M}^{(1)} & & \\ & \ddots & \\ & & \mathbf{M}^{(N_s)} \end{bmatrix} \begin{bmatrix} \ddot{\mathbf{u}}^{(1)} \\ \vdots \\ \ddot{\mathbf{u}}^{(N_s)} \end{bmatrix} + \begin{bmatrix} \mathbf{C}^{(1)} & & \\ & \ddots & \\ & & \mathbf{C}^{(N_s)} \end{bmatrix} \begin{bmatrix} \dot{\mathbf{u}}^{(1)} \\ \vdots \\ \dot{\mathbf{u}}^{(N_s)} \end{bmatrix} + \begin{bmatrix} \mathbf{K}^{(1)} & & \\ & \ddots & \\ & & \mathbf{K}^{(N_s)} \end{bmatrix} \begin{bmatrix} \mathbf{u}^{(1)} \\ \vdots \\ \mathbf{u}^{(N_s)} \end{bmatrix} = \begin{bmatrix} \mathbf{f}^{(1)} \\ \vdots \\ \mathbf{f}^{(N_s)} \end{bmatrix} + \begin{bmatrix} \mathbf{g}^{(1)} \\ \vdots \\ \mathbf{g}^{(N_s)} \end{bmatrix} \tag{2}$$

whereby the equations of the sth substructure can be isolated and subsequently rewritten in partitioned form as follows

$$\begin{bmatrix} \mathbf{M}_{ii}^{(s)} & \mathbf{M}_{ib}^{(s)} \\ \mathbf{M}_{bi}^{(s)} & \mathbf{M}_{bb}^{(s)} \end{bmatrix} \begin{bmatrix} \ddot{\mathbf{u}}_i^{(s)} \\ \ddot{\mathbf{u}}_b^{(s)} \end{bmatrix} + \begin{bmatrix} \mathbf{C}_{ii}^{(s)} & \mathbf{C}_{ib}^{(s)} \\ \mathbf{C}_{bi}^{(s)} & \mathbf{C}_{bb}^{(s)} \end{bmatrix} \begin{bmatrix} \dot{\mathbf{u}}_i^{(s)} \\ \dot{\mathbf{u}}_b^{(s)} \end{bmatrix} + \begin{bmatrix} \mathbf{K}_{ii}^{(s)} & \mathbf{K}_{ib}^{(s)} \\ \mathbf{K}_{bi}^{(s)} & \mathbf{K}_{bb}^{(s)} \end{bmatrix} \begin{bmatrix} \mathbf{u}_i^{(s)} \\ \mathbf{u}_b^{(s)} \end{bmatrix} = \begin{bmatrix} \mathbf{f}_i^{(s)} \\ \mathbf{f}_b^{(s)} \end{bmatrix} + \begin{bmatrix} \mathbf{0} \\ \mathbf{g}_b^{(s)} \end{bmatrix} \tag{3}$$

The superscript (s) in Eq. (3) denotes the quantities referring to the subdomain $\Omega^{(s)}$, $\mathbf{g}^{(s)} \in \mathbb{R}^{n^{(s)}}$ indicates the vector of internal forces at the interfaces, $n^{(s)}$ is the number of degrees of freedom of the sth substructure and the subscripts i and b refer to the internal $\mathbf{u}_i^{(s)} \in \mathbb{R}^{n_i^{(s)}}$ and boundary $\mathbf{u}_b^{(s)} \in \mathbb{R}^{n_b^{(s)}}$ degrees of freedom, respectively. The right-hand side of Eq. (3) is further simplified, containing only $\mathbf{g}_b^{(s)}$, for non-externally excited substructures whose dynamics are exclusively driven by the interface forces

In order to ensure equivalence between the initial model, described by Eq. (1), and the one obtained by dividing the domain into a number of uncoupled substructures, the latter should additionally satisfy the compatibility and equilibrium conditions. According to the former, any pair of connected degrees of freedom at the interface should have identical displace-

ment, while the latter requires that interface forces on connected degrees of freedom sum to zero. These can be written in compact form as

$$\mathbf{B}\tilde{\mathbf{u}}_b = \mathbf{0} \tag{4a}$$

$$\mathbf{L}^T\tilde{\mathbf{g}}_b = \mathbf{0} \tag{4b}$$

where $\tilde{\mathbf{u}}_b = \text{vec}\left(\left[\mathbf{u}_b^{(1)}\ \mathbf{u}_b^{(2)} \ldots \mathbf{u}_b^{(N_s)}\right]\right)$ and $\tilde{\mathbf{g}}_b = \text{vec}\left(\left[\mathbf{g}_b^{(1)}\ \mathbf{g}_b^{(2)} \ldots \mathbf{g}_b^{(N_s)}\right]\right)$, with vec(•) indicating the operator that stacks the matrices vertically, and the operators $\mathbf{B}$ and $\mathbf{L}$ are Boolean matrices, with the one representing the null space of the other, describing the connectivity of the substructures interface degrees of freedom.

In the context of structural dynamics, substructuring is typically used for the component-wise analysis of large-size and complex systems that are difficult and cumbersome to be processed as single entities. As such, the systems are partitioned into substructures, whose models are constructed independently and thereafter assembled in order to form the model of the total system, in either a primal or dual way. According to the former, a unique set of interface degrees of freedom is retained in Eq. (2), and the corresponding interface forces are eliminated through the equilibrium. This assembly is materialized by imposing the following constraint equation

$$\tilde{\mathbf{u}}_b = \mathbf{L}\mathbf{u}_b \tag{5}$$

where $\mathbf{u}_b \in \mathbb{R}^{n_b}$ is the unique set of interface degrees of freedom for the system represented by Eq. (1). On the contrary, the entire set of interface degrees of freedom is retained in a dual assembly, which is carried out by imposing the interface equilibrium as follows

$$\tilde{\mathbf{g}}_b = -\mathbf{B}^T\lambda \tag{6}$$

where λ are the Lagrange multipliers representing the interface force intensities.

In this contribution, the substructuring step is utilized for the independent modeling of system components, with the aim of devising a monitoring scheme able to circumvent the need of modelling the entire system, as graphically communicated in Fig. 1. In such formulation, the assembly step is also bypassed and the coupling of the substructure of interest with the rest of the system is achieved by fusing the former with measured structural response at the interfaces. For this reason, the superscript $\square^{(s)}$ is henceforth omitted and all symbols refer to a single substructure. A first step towards this end, comprises the order reduction of the substructure model, which is demonstrated in the following sections using the Craig-Bampton and Rubin methods. It should be noted that the applicability of the proposed framework is not limited to these two specific methods, but can be also fused with other substructuring and condensation works [30–35]. With the main difference among them consisting in the reduction ingredients, substructure methods can be classified into fixed- and free-interface approaches. Therefore, in order to highlight the specifics and advantages of each class, Craig-Bampton and Rubin methods are selected as the most indicative and widely used ones belonging to the fixed- and free-interface classes, respectively.

2.1. Fixed-interface methods

In the Craig-Bampton method [32], the partitioned equations of motion of the substructure, as established in Eq. (3), are reduced by introducing the following approximation for the internal displacement field

$$\mathbf{u}_i \approx \mathbf{\Phi}_i\mathbf{q}_i + \mathbf{\Psi}_b\mathbf{u}_b \tag{7}$$

in which $\mathbf{\Phi}_i \in \mathbb{R}^{n_i \times n_\phi}$ contains a truncated set of fixed-interface vibration modes, with $n_\phi \ll n_i$, and $\mathbf{q}_i \in \mathbb{R}^{n_\phi}$ is the corresponding modal coordinate vector. Such modes are obtained from the solution of the generalized eigenvalue problem related to the internal degrees of freedom

$$\left(\mathbf{K}_{ii} - \omega_{i,j}^2\mathbf{M}_{ii}\right)\phi_{i,j} = \mathbf{0} \tag{8}$$
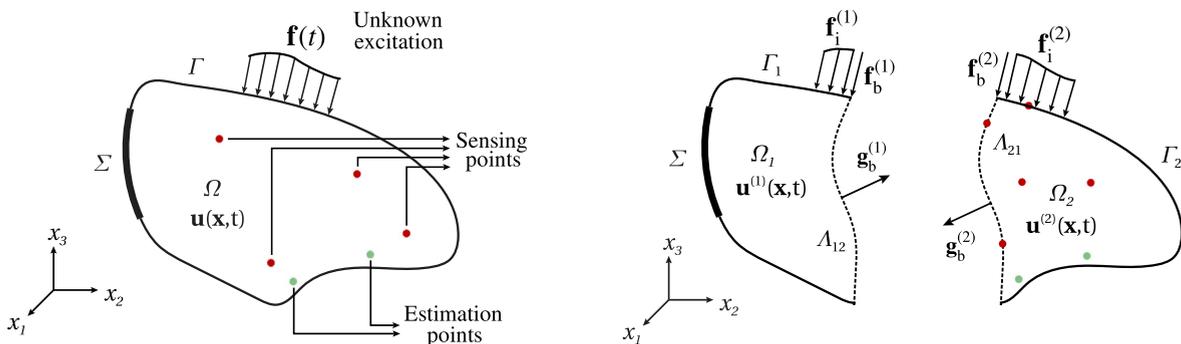
Fig. 1. Schematic representation of the full-domain (left) and substructure-based (right) problem of input-state estimation.

with $\omega_{i,j}$, for $j = 1, \ldots, n_\phi$ representing the associated eigenfrequencies. On the other hand, matrix $\Psi_b \in \mathbb{R}^{n_i \times n_b}$ contains the static constraint modes

$$\Psi_b = -\mathbf{K}_{ii}^{-1}\mathbf{K}_{ib} \tag{9}$$

which are obtained upon static condensation of the internal degrees of freedom of Eq. (3). Each one of these modes describes the static deformation of the internal part of the substructure when a unit displacement is applied to an interface degree of freedom and the remaining interface is kept restrained.

2.2. Free-interface methods

In contrast to the Craig-Bampton method, which is based on fixed-interface modes, free-interface methods,such as the Rubin and dual Craig-Bampton, are based on the vibration shapes obtained in absence of boundary conditions. These modes seem to be a more natural system or component feature since they can be experimentally extracted from a free-free vibration test. Under this assumption, the displacement field of the substructure is approximated as follows

$$\mathbf{u} \approx \Xi\mathbf{q}_f + \mathbf{R}\mathbf{q}_r + \Lambda\mathbf{g}_b \tag{10}$$

where $\Xi \in \mathbb{R}^{n \times n_f}$ is a truncated basis of free-free vibration modes, such that $n_f \ll n$, and $\mathbf{q}_f \in \mathbb{R}^{n_f}$ are the associated generalized coordinates. The former can be obtained by solving the eigenvalue problem associated with the full substructure matrices of Eq. (3), according to

$$\left(\mathbf{K} - \omega_{f,j}^2\mathbf{M}\right)\xi_j = \mathbf{0} \tag{11}$$

where $\omega_{f,j}$, for $j = 1, \ldots, n_f$, are the corresponding eigenfrequencies. The second term of Eq. (10) encompasses the rigid body motion of the substructure, whose computation is elaborated in the following subsection, with $\mathbf{R} \in \mathbb{R}^{n \times 6}$ and $\mathbf{q}_r \in \mathbb{R}^6$ representing the rigid body modes and amplitudes, respectively. Lastly, the third term of Eq. (10) represents the static effect of interface forces $\mathbf{g}_b \in \mathbb{R}^{n_b}$, which is mapped to the substructure through the residual attachment modes $\Lambda \in \mathbb{R}^{n \times n_b}$. For the sake of brevity, the derivation of such modes is herein omitted however, the reader is referred to [36,37] for a detailed explanation. It should be noted though that in analogy with the constraint modes, the residual attachment modes describe the displacement field of the substructure due to a unit force applied at the interface degrees of freedom and further satisfy the orthogonality conditions with respect to the mass and stiffness matrices.

By approximating the substructure displacements using Eq. (10), the generated reduced-order system is represented by a set of generalized coordinates $\mathbf{q}_f, \mathbf{q}_r$ and the interface forces $\mathbf{g}_b$. To allow for conventional assembly of this dual substructure representation with other components, such as physical substructures in the context of hybrid testing, Eq. (10) is further transformed in the context of Rubin method, in order to yield a displacement-based superelement. To do so, the interface forces need to be substituted by the associated displacements, and this is accomplished by partitioning Eq. (10) into two systems of equations, one referring to the internal degrees of freedom and a second one pertaining to the boundary quantities. Subsequently, solving the latter for interface displacements results in

$$\mathbf{g}_b = \mathbf{K}_{bb}^{(\Lambda)}(\mathbf{u}_b - \mathbf{R}_b\mathbf{q}_r - \Xi_b\mathbf{q}_f) \tag{12}$$

where subscript $_b$ denotes the submatrices referring to the boundary degrees of freedom and $\mathbf{K}_{bb}^{(\Lambda)} = \Lambda_b^{-1}$. Thereafter, the internal displacements can be expressed in terms of the generalized coordinates and the boundary displacements as follows

$$\mathbf{u}_i = \left(\Xi_i - \Lambda_i\mathbf{K}_{bb}^{(\Lambda)}\Xi_b\right)\mathbf{q}_f + \left(\mathbf{R}_i - \Lambda_i\mathbf{K}_{bb}^{(\Lambda)}\mathbf{R}_b\right)\mathbf{q}_r + \Lambda_i\mathbf{K}_{bb}^{(\Lambda)}\mathbf{u}_b \tag{13}$$

where similarly, subscript $_i$ designates the submatrices pertaining to internal displacements.

On the other hand, although the dual Craig-Bampton method is also based on the assumption that the total displacement field of the substructure is approximated by Eq. (10), the equations of motion are formulated on the basis of generalized displacements and boundary forces. In this sense, Eq. (10) is directly applied to transform Eq. (3) in the reduced space. Although such a formulation might not facilitate the assembly of reduced-order components, which is the goal in conventional substructure schemes, it provides an explicit expression for the sought for boundary forces in the context of inverse engineering.

2.2.1. Rigid body modes

In the context of substructuring, it might often be the case that a component is not constrained and as a result experiences rigid body modes, which represent displacement fields without deformation. Evidently, in the context of a forward simulation for the entire system, these modes would vanish upon assemblage of the substructures. However, they need be taken into account when a substructure is considered as a singleton in an inverse engineering context, where the measured response quantities might not be related to the deformation alone, as is the case with acceleration and inclination measurements. Although rigid body modes are inherently included in the Craig-Bampton scheme, they need to be additionally computed for the Rubin method, as well as for rigid interface reduction, which may be implemented with both methods. The extraction of such modes can be performed either by computing the nullspace of stiffness matrix or by solving the eigenvalue

problem of the unconstrained, i.e., free interface substructure and retaining the zero frequency eigenmodes. Alternatively, they can be efficiently obtained from the geometry of the structure by assembling the trace of each node as follows

$$\mathbf{R} = \begin{bmatrix} \mathbf{R}_1^T & \mathbf{R}_2^T & \ldots & \mathbf{R}_N^T \end{bmatrix}^T \tag{14}$$

For the general case of three-dimensional FE models with six degrees of freedom per node, the imprint of rigid modes on the nth node can be computed from the nodal coordinates

$$\mathbf{R}_n = [\mathbf{R}_{t,n} \quad \mathbf{R}_{r,n}] = \begin{bmatrix} \mathbf{I} & \mathbf{T}_{r,n} \\ \mathbf{0} & \mathbf{I} \end{bmatrix} \tag{15}$$

where $\mathbf{R}_{t,n} \in \mathbb{R}^{6 \times 3}$ represents the translational modes, indicated by the subscript $_t$, while $\mathbf{R}_{r,n} \in \mathbb{R}^{6 \times 3}$ contains the information related to the rotational modes, which is denoted by subscript $_r$. The coupling term $\mathbf{T}_{r,n} \in \mathbb{R}^{3 \times 3}$ for the calculation of displacements due to rotational modes may be obtained as follows

$$\mathbf{T}_{r,n} = \begin{bmatrix} 0 & (z_n - z_0) & -(y_n - y_0) \\ -(z_n - z_0) & 0 & (x_n - x_0) \\ (y_n - y_0) & -(x_n - x_0) & 0 \end{bmatrix} \tag{16}$$

where x_n, y_n and z_n, for $n = 1, \ldots N$, are the nodal coordinates while x_0, y_0 and z_0 designate the coordinates of a reference node on the substructure. By definition, the translational modes obtained from Eq. (15) are orthogonal to the mass matrix, and by extension to the stiffness matrix, however, this is not the case for the rotational modes since the reference point (x_0, y_0, z_0) can be arbitrarily chosen, without necessarily coinciding with the center of mass. In this sense, the rotational modes obtained from Eq. (15) need to be orthogonalized by removing the translational components from $\mathbf{R}_r$ through the following operation

$$\hat{\mathbf{R}}_r = \left(\mathbf{I} - \mathbf{R}_t \left(\mathbf{R}_t^T \mathbf{M} \mathbf{R}_t \right)^{-1} \mathbf{R}_t^T \mathbf{M} \right) \mathbf{R}_r \tag{17}$$

where $\mathbf{M}$ is the component mass matrix. Lastly, the orthogonalized with respect to mass and stiffness rotational modes can be assembled with the translational ones to form the normalized rigid body modes

$$\mathbf{R} = [\mathbf{R}_t \quad \hat{\mathbf{R}}_r] \mathbf{M}_R^{-1} \tag{18}$$

where $\mathbf{M}_R \in \mathbb{R}^{6 \times 6}$ is given by

$$\mathbf{M}_R = \mathrm{diag}(m_x, m_y, m_z, m_{r_x}, m_{r_y}, m_{r_z}) \tag{19}$$

and contains the inertial terms of both translational and rotational modes, which essentially represent the global inertial terms of the substructure.

2.3. Interface modes

Despite the significant order-reduction that may be achieved with the use of fixed- or free-interface modes for the internal displacements, the substructure dynamics represented by either Craig-Bampton or Rubin method are still described by the entire set of interface degrees of freedom. This set may be significantly large for sizable, or finely meshed interfaces, determining thus the computational efficiency of the overall substructure model [38]. The number of, either physical or generalized, interface degrees of freedom is an even more critical model aspect in the context of input estimation, where direct invertibility and problem conditioning are major concerns [39]. To this end, this section is focused on the interface reduction, with the aim of establishing a computationally efficient model, able to run in real time, which is further well conditioned and satisfies the conditions for direct invertibility.

2.3.1. Rigid reduction

The first approach for interface reduction is based on the assumption of stiff interfaces, whose behavior may be approximated by rigid body motions. Such an assumption reduces the interface kinematics, and subsequently the degrees of freedom, to only six components for a three-dimensional model, namely three translations and three rotations, implying thus the following transformation of boundary degrees of freedom

$$\mathbf{u}_b = \mathbf{\Gamma}_b \mathbf{q}_b \tag{20}$$

where $\mathbf{q}_b \in \mathbb{R}^{6 \times 1}$ is the vector of rigid body coordinates, given by $\mathbf{q}_b = [u_b, v_b, w_b, \theta_b, \phi_b, \psi_b]^T$, and $\mathbf{\Gamma}_b \in \mathbb{R}^{n_b \times 6}$ is the corresponding rigid body modes vector. The latter may be obtained from a node-basis approach, according to

$$\mathbf{\Gamma}_b = \mathrm{vec}(\mathbf{\Gamma}_{b,1} \, \mathbf{\Gamma}_{b,2} \, \ldots \, \mathbf{\Gamma}_{b,N}) \tag{21}$$

where $\mathbf{\Gamma}_{b,j} \in \mathbb{R}^{6 \times 6}$ for $j = 1, 2, \ldots, N$ represents the corresponding nodal vector of rigid motions, whose structure resembles the one of $\mathbf{R}_n$ defined in Eq. (15) and is given by

$$\boldsymbol{\Gamma}_{b,n} = \begin{bmatrix} \mathbf{I} & \mathbf{T}_{r,n} \\ \mathbf{0} & \mathbf{I} \end{bmatrix} \tag{22}$$

The coupling term $\mathbf{T}_{r,n} \in \mathbb{R}^{3 \times 3}$ between rotational and translational degrees of freedom is identical to the one defined in Eq. (16), with x_0, y_0 and z_0 indicating now the origin coordinates of the interface. Again, the origin may be placed to any position of the interface, without necessarily coinciding with existing nodes.

2.3.2. Modal reduction

When an interface is significantly flexible and therefore cannot be represented by rigid modes, the displacement field can be spanned by a set of generalized coordinates, which satisfy the eigenvalue problem

$$\left(\hat{\mathbf{K}}_{bb} - \omega_{b,k}^2 \hat{\mathbf{M}}_{bb} \right) \boldsymbol{\gamma}_{b,k} = \mathbf{0} \tag{23}$$

with $\boldsymbol{\gamma}_{b,k} \in \mathbb{R}^{n_b}$ denoting the kth interface mode and $\omega_{b,k}$ representing the corresponding eigenfrequency. The stiffness and mass terms $\hat{\mathbf{K}}_{bb}$ and $\hat{\mathbf{M}}_{bb}$ are obtained from the assembled interface matrices, which essentially comprise the stiffness and mass contribution from all connected substructures at the said interface. By retaining a truncated number of eigenmodes, as typically done in modal analysis, the displacement field of the interface may be described by

$$\mathbf{u}_b \approx \sum_{k=1}^{n_\gamma} \boldsymbol{\gamma}_{b,k} q_{b,k} = \boldsymbol{\Gamma}_b \mathbf{q}_b \tag{24}$$

where $\boldsymbol{\Gamma}_b \in \mathbb{R}^{n_b \times n_\gamma}$ contains the retained eigenvectors, whose dimension n_γ is typically significantly smaller than the initial number of degrees of freedom, so that $n_\gamma \ll n_b$.

2.4. Component-level reduction

Regardless of the substructuring approach, the physical degrees of freedom $\mathbf{u} \in \mathbb{R}^n$ can be transformed to a reduced space, wherein the substructure dynamics are represented by a set of generalized coordinates $\tilde{\mathbf{q}} \in \mathbb{R}^r$, such that $r \ll n$. Upon establishing the transformation matrix $\mathbf{T} \in \mathbb{R}^{n \times r}$ from the original to the reduced space, such that $\mathbf{u} = \mathbf{T}\mathbf{q}$, the reduction step may be carried out by means of a Galerkin projection, to yield the final form of reduced substructure equations

$$\tilde{\mathbf{M}}\ddot{\mathbf{q}} + \tilde{\mathbf{C}}\dot{\mathbf{q}} + \tilde{\mathbf{K}}\mathbf{q} = \tilde{\mathbf{f}} + \tilde{\mathbf{g}} \tag{25}$$

where the size and form of system matrices $\tilde{\mathbf{M}}, \tilde{\mathbf{C}}, \tilde{\mathbf{K}} \in \mathbb{R}^{r \times r}$ and force vectors $\tilde{\mathbf{f}}, \tilde{\mathbf{g}} \in \mathbb{R}^r$ depends on the substructure approach. To do so, the projection equation $\mathbf{u} = \mathbf{T}\mathbf{q}$ is initially substituted in Eq. (3), which gives rise to a residual term. The latter is subsequently enforced by the Galerkin condition to be orthogonal to the projection basis, yielding thus the reduced-order equations [40].

For proportionally, or Rayleigh, damped systems, which are considered in this work, the reduced damping matrix $\tilde{\mathbf{C}}$ is expressed as a linear combination of the reduced stiffness and mass matrices, $\tilde{\mathbf{C}} = \alpha \tilde{\mathbf{M}} + \beta \tilde{\mathbf{K}}$, with α and β designating the Rayleigh coefficients. The selection of these coefficients, at the level of component, is not straightforward however, in the applications to be demonstrated, the quality of input and state estimation is not affected by the amount of damping, similarly to what is observed in [10], when the latter lies in the regime of typical lightly-damped systems. As such, the coefficients are herein chosen such that the first two component-based modes are assigned the same amount of damping with the first two global vibration modes.

2.4.1. Fixed-interface method

For the Craig-Bampton method, the reduced space consists of the fixed-interface mode amplitudes $\mathbf{q}_i$ and the generalized interface coordinates $\mathbf{q}_b$, so that $\mathbf{q} = \text{vec}([\mathbf{q}_i \ \mathbf{q}_b]) \in \mathbb{R}^{n_\phi + n_\gamma}$. As such, the transformation to the reduced space may be established by combining Eq. (7) with either Eq. (20) or Eq. (23), depending on the interface reduction scheme, to yield the following expression

$$\begin{bmatrix} \mathbf{u}_i \\ \mathbf{u}_b \end{bmatrix} = \begin{bmatrix} \boldsymbol{\Phi}_i & \boldsymbol{\Psi}_b \boldsymbol{\Gamma}_b \\ \mathbf{0} & \boldsymbol{\Gamma}_b \end{bmatrix} \begin{bmatrix} \mathbf{q}_i \\ \mathbf{q}_b \end{bmatrix} = \mathbf{T}\mathbf{q} \tag{26}$$

and subsequently derive the reduced equations of motion by means of a Galerkin projection

$$\begin{bmatrix} \mathbf{I} & \boldsymbol{\Phi}_i^T (\mathbf{M}_{ib} + \mathbf{M}_{ii} \boldsymbol{\Psi}_b) \boldsymbol{\Gamma}_b \\ \boldsymbol{\Gamma}_b^T (\boldsymbol{\Psi}_b^T \mathbf{M}_{ii} + \mathbf{M}_{bi}) \boldsymbol{\Phi}_i & \boldsymbol{\Gamma}_b^T (\mathbf{M}_{bb} + \mathbf{M}_{bi} \boldsymbol{\Psi}_b + \boldsymbol{\Psi}_b^T \mathbf{M}_{ib} + \boldsymbol{\Psi}_b^T \mathbf{M}_{ii} \boldsymbol{\Psi}_b) \boldsymbol{\Gamma}_b \end{bmatrix} \begin{bmatrix} \ddot{\mathbf{q}}_i \\ \ddot{\mathbf{q}}_b \end{bmatrix} + \begin{bmatrix} \boldsymbol{\Omega}_i^2 & \mathbf{0} \\ \mathbf{0} & \boldsymbol{\Omega}_b^2 \end{bmatrix} \begin{bmatrix} \mathbf{q}_i \\ \mathbf{q}_b \end{bmatrix} = \begin{bmatrix} \tilde{\mathbf{f}}_i \\ \tilde{\mathbf{f}}_b \end{bmatrix} + \begin{bmatrix} \mathbf{0} \\ \tilde{\mathbf{g}}_b \end{bmatrix} \tag{27}$$

where $\boldsymbol{\Omega}_i \in \mathbb{R}^{n_\phi \times n_\phi}$ and $\boldsymbol{\Omega}_b \in \mathbb{R}^{n_\gamma \times n_\gamma}$ are the diagonal matrices containing the eigenfrequencies of the fixed-interface and interface vibration modes, respectively. Lastly, it should be noted that when the interface degrees of freedom are modally

reduced, the corresponding eigenfrequencies are directly extracted from Eq. (23), while in the case of rigid reduction, $\mathbf{\Omega}_b^2$ may be computed as

$$\mathbf{\Omega}_b^2 = \mathbf{\Gamma}_b^T(\mathbf{K}_{bb} + \mathbf{K}_{bi}\mathbf{\Psi}_b)\mathbf{\Gamma}_b \tag{28}$$

which is derived from the analytical transformation of Eq. (3) using Eq. (26). The generalized force terms on the right-hand side of Eq. (27), are given by

$$\tilde{\mathbf{f}}_i = \mathbf{\Phi}_i^T\mathbf{f}_i \tag{29a}$$

$$\tilde{\mathbf{f}}_b = \mathbf{\Gamma}_b^T\mathbf{\Psi}_{bb}^T\mathbf{f}_i + \mathbf{\Gamma}_b^T\mathbf{f}_b \tag{29b}$$

$$\tilde{\mathbf{g}}_b = \mathbf{\Gamma}_b^T\mathbf{g}_b \tag{29c}$$

2.4.2. Free-interface method

In Rubin method the physical degrees of freedom are projected to a reduced space, which consists of the free-interface modal coordinates $\mathbf{q}_f$, the interface mode amplitudes $\mathbf{q}_b$ and the rigid body coordinates $\mathbf{q}_r$, so that $\mathbf{q} = \mathrm{vec}([\mathbf{q}_f\ \mathbf{q}_b\ \mathbf{q}_r]) \in \mathbb{R}^{n_f+n_\gamma+6}$. Accordingly, the transformation can be constructed by combining Eq. (13) with either Eq. (20) or Eq. (23), yielding thus the following relation between physical and generalized degrees of freedom

$$\begin{bmatrix} \mathbf{u}_i \\ \mathbf{u}_b \end{bmatrix} = \begin{bmatrix} \mathbf{\Xi}_i - \mathbf{\Lambda}_i\mathbf{K}_{bb}^{(\Lambda)}\mathbf{\Xi}_b & \mathbf{\Lambda}_i\mathbf{K}_{bb}^{(\Lambda)}\mathbf{\Gamma}_b & \mathbf{R}_i - \mathbf{\Lambda}_i\mathbf{K}_{bb}^{(\Lambda)}\mathbf{R}_b \\ \mathbf{0} & \mathbf{\Gamma}_b & \mathbf{0} \end{bmatrix}\begin{bmatrix} \mathbf{q}_f \\ \mathbf{q}_b \\ \mathbf{q}_r \end{bmatrix} = \mathbf{T}\mathbf{q} \tag{30}$$

where subscripts $_{i,b}$ indicate the submatrices pertaining to the internal and boundary degrees of freedom, respectively. Subsequently, the Rubin-based reduced-order system is obtained by means of a Galerkin projection, as follows

$$\begin{bmatrix} \mathbf{I}+\mathbf{\Xi}_b^T\hat{\mathbf{M}}_{bb}^{(\Lambda)}\mathbf{\Xi}_b & -\mathbf{\Xi}_b^T\hat{\mathbf{M}}_{bb}^{(\Lambda)}\mathbf{\Gamma}_b & \mathbf{\Xi}_b^T\hat{\mathbf{M}}_{bb}^{(\Lambda)}\mathbf{R}_b \\ -\mathbf{\Gamma}_b^T\hat{\mathbf{M}}_{bb}^{(\Lambda)}\mathbf{\Xi}_b & \mathbf{\Gamma}_b^T\mathbf{M}_{bb}^{(\Lambda)}\mathbf{\Gamma}_b & -\mathbf{\Gamma}_b^T\hat{\mathbf{M}}_{bb}^{(\Lambda)}\mathbf{R}_b \\ \mathbf{R}_b^T\hat{\mathbf{M}}_{bb}^{(\Lambda)}\mathbf{\Xi}_b & -\mathbf{R}_b^T\hat{\mathbf{M}}_{bb}^{(\Lambda)}\mathbf{\Gamma}_b & \mathbf{I}+\mathbf{R}_b^T\hat{\mathbf{M}}_{bb}^{(\Lambda)}\mathbf{R}_b \end{bmatrix}\begin{bmatrix} \ddot{\mathbf{q}}_f \\ \ddot{\mathbf{q}}_b \\ \ddot{\mathbf{q}}_r \end{bmatrix} + \begin{bmatrix} \mathbf{\Omega}_f^2+\mathbf{\Xi}_b^T\mathbf{K}_{bb}^{(\Lambda)}\mathbf{\Xi}_b & -\mathbf{\Xi}_b^T\mathbf{K}_{bb}^{(\Lambda)}\mathbf{\Gamma}_b & \mathbf{\Xi}_b^T\mathbf{K}_{bb}^{(\Lambda)}\mathbf{R}_b \\ -\mathbf{\Gamma}_b^T\mathbf{K}_{bb}^{(\Lambda)}\mathbf{\Xi}_b & \mathbf{\Gamma}_b^T\mathbf{K}_{bb}^{(\Lambda)}\mathbf{\Gamma}_b & -\mathbf{\Gamma}_b^T\mathbf{K}_{bb}^{(\Lambda)}\mathbf{R}_b \\ \mathbf{R}_b^T\mathbf{K}_{bb}^{(\Lambda)}\mathbf{\Xi}_b & -\mathbf{R}_b^T\mathbf{K}_{bb}^{(\Lambda)}\mathbf{\Gamma}_b & \mathbf{R}_b^T\mathbf{K}_{bb}^{(\Lambda)}\mathbf{R}_b \end{bmatrix}\begin{bmatrix} \mathbf{q}_f \\ \mathbf{q}_b \\ \mathbf{q}_r \end{bmatrix} = \begin{bmatrix} \tilde{\mathbf{f}}_f \\ \tilde{\mathbf{f}}_b \\ \tilde{\mathbf{f}}_r \end{bmatrix} + \begin{bmatrix} \mathbf{0} \\ \tilde{\mathbf{g}}_b \\ \mathbf{0} \end{bmatrix} \tag{31}$$

where $\mathbf{M}_{bb}^{(\Lambda)} = \mathbf{\Lambda}^T\mathbf{M}\mathbf{\Lambda}$ and $\hat{\mathbf{M}}_{bb}^{(\Lambda)} = \mathbf{K}_{bb}^{(\Lambda)}\mathbf{M}_{bb}^{(\Lambda)}\mathbf{K}_{bb}^{(\Lambda)}, \mathbf{\Omega}_f \in \mathbb{R}^{n_f \times n_f}$ is the diagonal matrix of free-free eigenfrequencies, while the generalized force vectors are expressed as

$$\tilde{\mathbf{f}}_f = \left(\mathbf{\Xi}_i^T - \mathbf{\Xi}_b^T\mathbf{K}_{bb}^{(\Lambda)}\mathbf{\Lambda}_i^T\right)\mathbf{f}_i \tag{32a}$$

$$\tilde{\mathbf{f}}_b = \mathbf{\Gamma}_b^T\mathbf{K}_{bb}^{(\Lambda)}\mathbf{\Lambda}_i^T\mathbf{f}_i + \mathbf{\Gamma}_b^T\mathbf{f}_b \tag{32b}$$

$$\tilde{\mathbf{f}}_r = \left(\mathbf{R}_i^T - \mathbf{R}_b^T\mathbf{K}_{bb}^{(\Lambda)}\mathbf{\Lambda}_i^T\right)\mathbf{f}_i \tag{32c}$$

$$\tilde{\mathbf{g}}_b = \mathbf{\Gamma}_b^T\mathbf{g}_b \tag{32d}$$

3. Input-state estimation

By introducing the state vector $\mathbf{x} = \mathrm{vec}([\mathbf{q}\ \dot{\mathbf{q}}]) \in \mathbb{R}^{2n}$, the reduced-order governing equations of motion of a substructure, given in the general case by Eq. (25) and in particular by Eq. (27) for the Craig-Bampton method or Eq. (31) for the Rubin method, can be transformed into a state-space representation

$$\dot{\mathbf{x}} = \mathbf{A}_c\mathbf{x} + \mathbf{B}_c\mathbf{p} \tag{33a}$$

$$\mathbf{y} = \mathbf{G}_c\mathbf{x} + \mathbf{J}_c\mathbf{p} \tag{33b}$$

where $\mathbf{y} \in \mathbb{R}^{n_y}$ denotes the observed system outputs and $\mathbf{p} \in \mathbb{R}^{n_p}$ indicates the driving forces. Assuming that no external loads are exerted on the interfaces, i.e., $\mathbf{f}_b = \mathbf{0}$, the substructure dynamics are either driven by the internal interface forces $\mathbf{g}_b$ or additionally by the external loads $\mathbf{f}_i$ acting on the internal degrees of freedom, The latter is typically a sparse vector, which contains the inputs $\mathbf{p}_i \in \mathbb{R}^{n_{p_i}}$ that are exerted on a limited number of locations, so that $\mathbf{f}_i = \mathbf{S}_{p_i}\mathbf{p}_i$, with $\mathbf{S}_{p_i} \in \mathbb{R}^{n_i \times n_{p_i}}$ being a boolean matrix. Therefore, the matrices of state equation, which are derived from the equations of motion, are written as follows

$$\mathbf{A}_c = \begin{bmatrix} \mathbf{0} & \mathbf{I} \\ -\tilde{\mathbf{M}}^{-1}\tilde{\mathbf{K}} & -\tilde{\mathbf{M}}^{-1}\tilde{\mathbf{C}} \end{bmatrix}, \mathbf{B}_c = \begin{bmatrix} \mathbf{0} \\ \tilde{\mathbf{M}}^{-1}\tilde{\mathbf{T}}^T \end{bmatrix} \tag{34}$$

where $\bar{\mathbf{T}}$ is the input transformation matrix, whose structure depends on whether the substructure dynamics are driven only by interface forces, or both by interface and external loads. In the general case, $\bar{\mathbf{T}}^{\mathrm{T}}$ is the transpose of the reduction matrix $\mathbf{T}$, which may be obtained either by Eq. (26) or by Eq. (30), for Craig-Bampton and Rubin methods, respectively. However, it is herein slightly modified, in order to reduce the number of identified forces, according to the discussion of the previous paragraph. Thus, the form of $\bar{\mathbf{T}}^{\mathrm{T}}$ for each one of the two loading cases and for each one of the substructure methods is presented in Table 1, where it can be seen that the interface forces are not obtained by directly estimating $\mathbf{g}_{\mathrm{b}}$ as such, but through the estimation of the generalized interface forces $\tilde{\mathbf{g}}_{\mathrm{b}}$.

The structure of output influence and direct transmission matrices, $\mathbf{G}_{\mathrm{c}}$ and $\mathbf{J}_{\mathrm{c}}$ respectively, is dictated by the measured response quantities, which for typical civil engineering systems consist of displacements, usually in the form of inclination measurements, as well as accelerations and strains, yielding thus the following expressions

$$\mathbf{G}_{\mathrm{c}} = \begin{bmatrix} \mathbf{S}_{\mathrm{d}}\mathbf{T} & \mathbf{0} \\ \mathbf{S}_{\mathrm{a}}\mathbf{T}\tilde{\mathbf{M}}^{-1}\tilde{\mathbf{K}} & \mathbf{S}_{\mathrm{a}}\mathbf{T}\tilde{\mathbf{M}}^{-1}\tilde{\mathbf{C}} \\ \mathbf{D}_{\mathrm{e}}\,\mathbf{S}_{\mathrm{d},\epsilon}\mathbf{T} & \mathbf{0} \end{bmatrix}, \quad \mathbf{J}_{\mathrm{c}} = \begin{bmatrix} \mathbf{0} \\ \mathbf{S}_{\mathrm{a}}\mathbf{T}\tilde{\mathbf{M}}^{-1}\bar{\mathbf{T}}^{\mathrm{T}} \\ \mathbf{0} \end{bmatrix} \tag{35}$$

where $\mathbf{S}_{\mathrm{d}} \in \mathbb{R}^{n_{\mathrm{d}}}$ and $\mathbf{S}_{\mathrm{a}} \in \mathbb{R}^{n_{\mathrm{a}}}$ are selection matrices for displacements and accelerations and $\mathbf{S}_{\mathrm{d},\epsilon} \in \mathbb{R}^{n_{\epsilon}}$ denotes the selection matrix for displacements related to strain measurements. In the context of Finite Element modeling, where strains are retrieved at the element level, $\mathbf{S}_{\mathrm{d},\epsilon}$ selects the system displacements that correspond to the element nodal degrees of freedom. Thereafter, the displacements are transformed into strains through the block-diagonal matrix $\mathbf{D}_{\mathrm{e}}$, which contains the element deformation matrices.

By temporal discretization of the state-space model of Eqs. (33) with a sampling rate of $1/\Delta t$, and upon adding the noise terms $\mathbf{w}_k$ and $\mathbf{v}_k$, which represent the modeling and measurement errors respectively, the discrete-time stochastic state-space model is obtained as

$$\mathbf{x}_{k+1} = \mathbf{A}\mathbf{x}_k + \mathbf{B}\mathbf{p}_k + \mathbf{w}_k \tag{36a}$$
$$\mathbf{y}_k = \mathbf{G}\mathbf{x}_k + \mathbf{J}\mathbf{p}_k + \mathbf{v}_k \tag{36b}$$

where both $\mathbf{w}_k \in \mathbb{R}^{2n}$ and $\mathbf{v}_k \in \mathbb{R}^{n_y}$ are zero-mean Gaussian processes with known covariance matrices $\mathbf{Q}^{\mathrm{w}} = \mathbb{E}[\mathbf{w}_k\mathbf{w}_l^{\mathrm{T}}]$ and $\mathbf{Q}^{\mathrm{v}} = \mathbb{E}[\mathbf{v}_k\mathbf{v}_l^{\mathrm{T}}]$. The discrete-time system matrices are accordingly obtained through a zero-order hold scheme as: $\mathbf{A} = e^{\mathbf{A}_{\mathrm{c}}\Delta t}$, $\mathbf{B} = [\mathbf{A} - \mathbf{I}]\mathbf{A}_{\mathrm{c}}^{-1}\mathbf{B}_{\mathrm{c}}$, $\mathbf{G} = \mathbf{G}_{\mathrm{c}}$ and $\mathbf{J} = \mathbf{J}_{\mathrm{c}}$.

A number of recursive Bayesian approaches [7–9] has been recently proposed and implemented for jointly estimating the input and state of structural systems on the basis of the state-space model described by Eqs. (36). Although the estimation quality is reported to be dependent on the implemented algorithm [11,41], this paper is focused on establishing and underlining the specifics of a component-based vibration monitoring scheme. As such, the results presented in the following section are indicatively generated with the Augmented Kalman filter (AKF), where the state vector $\mathbf{x}_k$ is augmented with the inputs $\mathbf{p}_k$, to form the augmented state vector $\mathbf{z}_k = \mathrm{vec}([\mathbf{x}_k \ \mathbf{p}_k])$. In such a context, it is additionally postulated that the input evolution can be captured by a random-walk process

$$\mathbf{p}_{k+1} = \mathbf{p}_k + \mathbf{r}_k \tag{37}$$

where $\mathbf{r}_k \in \mathbb{R}^{n_{\mathrm{p}}}$ denotes the zero-mean white Gaussian noise term, with $\mathbf{Q}^{\mathrm{pp}} = \mathbb{E}[\mathbf{p}_k\mathbf{p}_l^{\mathrm{T}}]$ representing the corresponding covariance matrix. It should be noted that although the estimation is herein performed using the AKF, any other form of Bayesian filter for state and input estimation, with different assumptions on the evolution of the latter [42,43], may be well tailored to the proposed methodology.

Table 1
Input transformation matrix for systems driven i) only by interface and ii) both by interface and external forces.

Method	$\mathbf{p} = \tilde{\mathbf{g}}_{\mathrm{b}}$	$\mathbf{p} = [\mathbf{p}_{\mathrm{i}}^{\mathrm{T}} \ \tilde{\mathbf{g}}_{\mathrm{b}}^{\mathrm{T}}]^{\mathrm{T}}$
Fixed-interface	$\bar{\mathbf{T}}^{\mathrm{T}} = \begin{bmatrix} \mathbf{0} \\ \mathbf{I} \end{bmatrix}$	$\bar{\mathbf{T}}^{\mathrm{T}} = \begin{bmatrix} \mathbf{\Phi}_{\mathrm{i}}^{\mathrm{T}}\mathbf{S}_{\mathrm{p}_{\mathrm{i}}} & \mathbf{0} \\ \mathbf{\Gamma}_{\mathrm{b}}^{\mathrm{T}}\mathbf{\Psi}_{\mathrm{b}}^{\mathrm{T}}\mathbf{S}_{\mathrm{p}_{\mathrm{i}}} & \mathbf{I} \end{bmatrix}$
Free-interface	$\bar{\mathbf{T}}^{\mathrm{T}} = \begin{bmatrix} \mathbf{0} \\ \mathbf{I} \\ \mathbf{0} \end{bmatrix}$	$\bar{\mathbf{T}}^{\mathrm{T}} = \begin{bmatrix} \left(\mathbf{\Xi}_{\mathrm{i}}^{\mathrm{T}} - \mathbf{\Xi}_{\mathrm{b}}^{\mathrm{T}}\mathbf{K}_{\mathrm{bb}}^{(\Lambda)}\mathbf{\Lambda}_{\mathrm{i}}^{\mathrm{T}}\right)\mathbf{S}_{\mathrm{p}_{\mathrm{i}}} & \mathbf{0} \\ \mathbf{\Gamma}_{\mathrm{b}}^{\mathrm{T}}\mathbf{K}_{\mathrm{bb}}^{(\Lambda)}\mathbf{\Lambda}_{\mathrm{i}}^{\mathrm{T}}\mathbf{S}_{\mathrm{p}_{\mathrm{i}}} & \mathbf{I} \\ \left(\mathbf{R}_{\mathrm{i}}^{\mathrm{T}} - \mathbf{R}_{\mathrm{b}}^{\mathrm{T}}\mathbf{K}_{\mathrm{bb}}^{(\Lambda)}\mathbf{\Lambda}_{\mathrm{i}}^{\mathrm{T}}\right)\mathbf{S}_{\mathrm{p}_{\mathrm{i}}} & \mathbf{0} \end{bmatrix}$

Algorithm 1: Selection of reduction basis components

    Input : Candidate basis components $[\mathbf{v}_1, \mathbf{v}_2, ..., \ldots, \mathbf{v}_m]$

    Output: Reduction basis $\mathbf{V}$

1   Run the reference model ;

2   Initialize $\mathbf{V} \leftarrow \mathbf{V}^{(0)}$, MSE $\leftarrow$ MSE$^{(0)}$;

3   **for** $n = 1$ **to** m **do**

4   Construct ROM $\mathcal{M}_n([\mathbf{V}\ \mathbf{v}_n]) = \left\{ \tilde{\mathbf{M}},\ \tilde{\mathbf{C}},\ \tilde{\mathbf{K}},\ \mathbf{T},\ \bar{\mathbf{T}} \right\}$;

5   Construct state-space $\mathcal{S}_n(\mathcal{M}_n) = \{\mathbf{A},\ \mathbf{B},\ \mathbf{C},\ \mathbf{D},\ \Delta t\}$;

6   Initialize output sequence $\mathbf{Y}^{(n)} \leftarrow \mathbf{0}$;

7   **for** $k = 1$ **to** N **do**

8   Run input-state estimation steps ;

9   Calculate output prediction $\hat{\mathbf{y}}_k^{(n)}$;

10        $\mathbf{Y}_k^{(n)} \leftarrow \hat{\mathbf{y}}_k^{(n)}$;

11   **end**

12   MSE$^{(n)} \leftarrow \sum_{k=1}^{N} \left\| \mathbf{Y}_k - \mathbf{Y}_k^{(n)} \right\|^2$;

13   **if** $\dfrac{\text{MSE} - \text{MSE}^{(n)}}{\text{MSE}} \geq$ tol **then**

14        $\mathbf{V} \leftarrow [\mathbf{V}\ \mathbf{v}_n]$, MSE $\leftarrow$ MSE$^{(n)}$;

15   **end**

16   **end**

One of the major concerns arising in the proposed framework is the selection of the reduction order and by extension, the components forming the reduction basis $\mathbf{V} \in \{\boldsymbol{\Xi}, \boldsymbol{\Phi}, \boldsymbol{\Gamma}_{\mathrm{b}}\}$. In a forward substructure problem the reduction basis of each component is chosen such that the dynamic properties of the assembled system are well retained within a specific frequency range. However, this is not applicable in an inverse context where the substructure model is utilized to locally represent the system dynamics. When information from forward simulations of the entire system is available, this can be exploited for the construction of the reduction basis. In the absence however of such information, which is often the case when a model of the entire system is not readily available, the order may be determined on the basis of the mean square error (MSE)

$$\text{MSE} = \frac{1}{N} \sum_{k=1}^{N} \|\mathbf{y}_k - \hat{\mathbf{y}}_k\| \tag{38}$$

which need be evaluated for a number of candidate models $\mathcal{M}_n$ with different reduction bases $\mathbf{V}^{(n)}$. Concretely, the input-state estimation problem is initially solved using a reference Reduced Order Model (ROM) $\mathcal{M}_0(\mathbf{V}^{(0)})$, with $\mathbf{V}^{(0)}$ being the underlying reference reduction basis, in order to extract the predicted output sequence $\mathbf{Y}^{(0)} = \left[\mathbf{y}_1^{(0)}\ \mathbf{y}_2^{(0)}\ \cdots\ \mathbf{y}_N^{(0)} \right]$ for a number of validation points and subsequently compute the corresponding mean square error MSE$^{(0)}$. Thereafter, the ROM is reevaluated by appending the first candidate component $\mathbf{v}_1$ on the reduction basis, so that $\mathbf{V}^{(1)} = \left[\mathbf{V}^{(0)}\ \mathbf{v}_1 \right]$, and then the mean square error MSE$^{(1)}$ obtained using $\mathcal{M}_1\left(\mathbf{V}^{(1)}\right)$ is used as a metric for the significance of $\mathbf{v}_1$. Therefore, if $\mathcal{M}_1\left(\mathbf{V}^{(1)}\right)$ scores a better mean square error, within a certain tolerance, than the previous best, $\mathbf{v}_1$ is retained in the reduction basis and the best MSE is updated, otherwise $\mathbf{v}_1$ is discarded. The algorithm then proceeds to the assessment of the next component until all candidates $\mathbf{v}_n$, for $n = 1, 2, \ldots, m$, are examined. The detailed steps for selecting the reduction basis components are documented in Algorithm 1.

It should be noted that the range of candidate components for the reduction basis is subjected to certain observability limitations, which are imposed by the number and location of output measurements. Concretely, it must be ensured that the state-space model $\mathcal{S}_n(\mathcal{M}_n)$ derived for each ROM $\mathcal{M}_n\left(\mathbf{V}^{(n)}\right)$ is observable. By generalizing the discrete-time observability conditions for modally reduced systems [39], it is implied that for a reduced-order substructure model none of the terms $\mathbf{S}_{\mathrm{d}}\mathbf{T}, \mathbf{S}_{\mathrm{a}}\mathbf{T}$ and $\mathbf{S}_{\mathrm{d,\epsilon}}\mathbf{T}$, appearing in the measurement equation, contains any zero columns. Furthermore, it might be, depending

on the problem dynamics, that the error metric is notably reduced by assessing two candidate components together, than separately. In that case, a slight modification of Algorithm 1 would be required in order to assess the combinatorial score of candidate basis vectors. Such an effect has not been observed in the considered applications, hence the proposed algorithm. Lastly, it should be underlined that in the context of generalized input estimation, an increase in the number of basis components might also imply an increase in the number of inputs to be estimated, with the latter being bounded, due to stability reasons, by the number of strain/displacement measurements.

4. Case studies

In what follows, the proposed framework is demonstrated through simulated examples of WT structures, whereby the NREL 5.0 MW land-based turbine is simulated under operational conditions and the full-field vibration response and interface, as well as external forces at major components, i.e., tower and blades, are estimated on the basis of a limited number of output-only measurements. For a detailed description of the NREL 5.0 MW structural properties, the reader is referred to [44]. The considered WT system is modeled using FAST v8 in order to perform a number of aero-servo-elastic simulations, which serve for the extraction of synthetic vibration data. In order to loosely illustrate the robustness of the method, each one of the following case studies represents a different operating point of the WT, which is defined by the mean wind speed, sampled from a Weibull distribution with mean equal to 11 m/s, and the corresponding turbulence, drawn from a conditional on the mean wind speed lognormal distribution.

The motivation for establishing such a case study stems from the large degree of uncertainty that characterizes the dynamic response of operating WTs, which constitutes a limiting factor for the implementation of a global response identification framework. Therefore, in order to reduce this uncertainty, which is primarily associated with the aerodynamic loads and the various mechanical parts at the level of nacelle, and to further circumvent the construction of an entire WT model, which constitutes a considerably laborious task and involves the modeling of intricate and time-varying dynamics, the identification process may be carried out using the proposed substructure framework. The components of interest can be thus modeled separately and thereafter coupled with the rest of the system through the measured and estimated interface quantities.

4.1. Case A: wind turbine tower

The first case study is focused on the vibration monitoring of the NREL 5 MW WT. To this end, the entire WT is first simulated in order to obtain operational response measurements at the virtual sensing points, which are illustrated in Fig. 2(a) and (b) with red dots. Thereafter, the input and state are jointly estimated at the tower substructure, which is depicted in Fig. 2(c). Since the wind loads acting on the tower, i.e., drag forces bear only a minor contribution to the global dynamics [45,46] under normal operational conditions, it is herein assumed that the dynamics of the tower are exclusively driven by the top interface forces. The effect of distributed drag load on the tower, which might be more pronounced in parked

(a) Forward simulation   (b) Response measurements   (c) Inverse problem
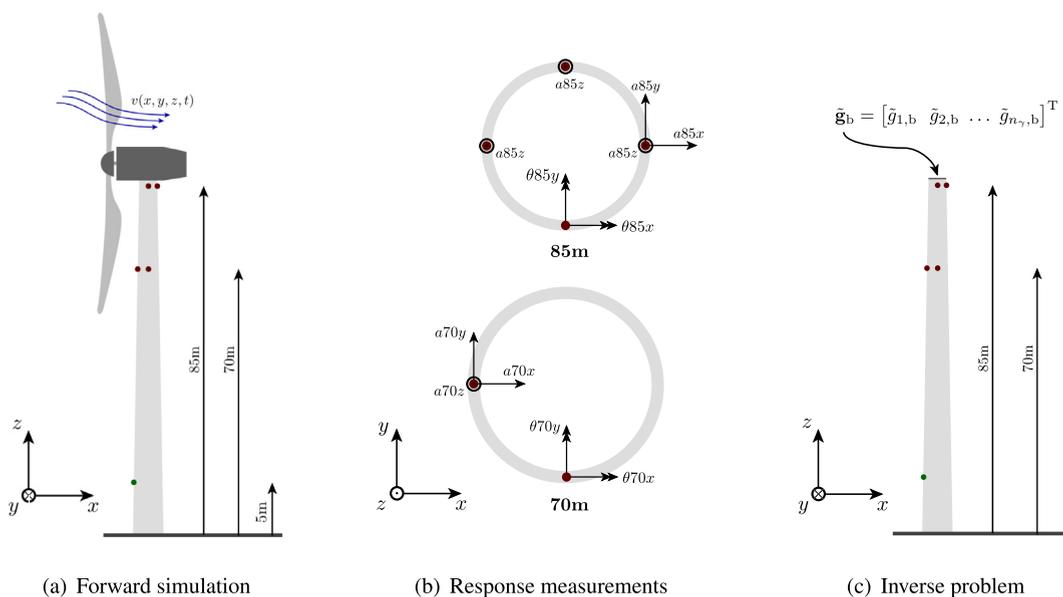
Fig. 2. Tower model; red points represent the measurement locations; green dots are the estimation/validation points.

or idling conditions, can be further included in terms of the generalized forces, similarly to the blade aerodynamic loads of the third case study.

As previously mentioned, the measurement data are generated using FAST v8 however, the substructure is represented by a three-dimensional shell FE model, so as to ensure the independence from the forward simulator. The substructure full-order model consists of 28,300 shell elements and 170,400 degrees of freedom, with the bottom cross-section being fixed and the top one considered as an interface. The model is reduced using both Craig-Bampton and Rubin methods to 8 generalized coordinates, with the selection of these components relying on the requirement that the entire reduction basis spans the space of the first two vibration modes of the WT, as suggested by existing knowledge on WT tower dynamics [47]. In the first case the reduced-order model comprises the first dynamically important [48] fixed-interface mode in each transverse direction, while the Rubin-reduced model is similarly composed of the first free-interface components in x and y directions. Lastly, in both cases the tower-top interface is modally reduced, with the first 8 vibration modes depicted in Fig. 3.

It should be noted that although the type of interface reduction, i.e., rigid or modal, depends on the geometry and stiffness of the interface, the number of generalized forces to be identified is mainly dictated by invertibility, stability and uniqueness conditions [49,39]. These are in turn directly associated with the size n_γ of the interface reduction basis, as well as with the number of displacement/strain and acceleration measurements. Concretely, the number of identified interface forces can exceed neither the size of the corresponding basis nor the number of acceleration measurements referring to the interface, while it is further limited by the number of displacements and/or strain sensors for stability and uniqueness of the inversion.

In the present application, where interface forces are estimated in terms of the generalized coordinates, their number cannot be by definition smaller than or equal to n_γ. Thereafter, with the adopted sensor layout shown in Fig. 2, stability and uniqueness are ensured by retaining and therefore estimating only the first six generalized degrees of freedom, whose corresponding shapes are depicted in Fig. 3 and essentially represent a rigid reduction. Although higher-order interface modes are not important for WT towers, which are well described by the kinematics of beam theory, they could be included in the estimation of blade interface forces, where warping effects are significant. In that case, additional sensing points would be required to meet the above conditions and ensure that the rank of term $\mathbf{S}_a \mathbf{T} \tilde{\mathbf{M}}^{-1} \tilde{\mathbf{T}}^T$ from the feedthrough matrix $\mathbf{J}$ defined in Eq. (35), where $\mathbf{T}$ is obtained either by Eq. (26) or Eq. (30), is equal to the number of generalized forces.

The assessment of the proposed approach is performed in terms of the estimated substructure state, whose accuracy is reflected through the predicted response at unmeasured locations (Fig. 2), as well as through the accuracy of the estimated interface forces. Regarding the latter, it should be underlined that such estimates do not constitute any type of equivalent force [26], but represent the ones actually driving the tower response and essentially reflect the unaccounted-for system dynamics. The simulation outputs are initially corrupted with 3% Gaussian white noise and the estimation results are obtained using a diagonal covariance matrix for the input process noise, whose values are listed in Table 2. Fig. 4 illustrates the time histories of the estimated vibration response at the validation points, using both Craig-Bampton and Rubin methods, along with the actual values. It can be seen that although the dynamics of the rotor are not included in the identification process, the response at unmeasured locations is estimated with sufficient accuracy.

As mentioned already in Section 3 and discussed in the previous paragraphs, the input estimation is performed in terms of the generalized forces $\tilde{\mathbf{g}}_b$, whose estimates are presented and compared with the actual values in Fig. 5. Once these are successfully estimated, the corresponding nodal interface forces can be subsequently retrieved according to

$$\mathbf{g}_b = \mathbf{\Gamma}_b (\mathbf{\Gamma}_b^T \mathbf{\Gamma}_b)^{-1} \tilde{\mathbf{g}}_b = (\mathbf{\Gamma}_b^T)^\dagger \tilde{\mathbf{g}}_b \qquad (39)$$

where $\square^\dagger$ denotes the pseudo-inverse operator. In this case study, the proposed approach is implemented for a single component and therefore retrieval of the interface forces in nodal space might not be of interest. However, a natural extension of the approach would include more than one component, as is the case for instance in hybrid testing applications, in which one part of the system is experimentally tested while the rest is numerically modeled and therefore the retrieval of nodal forces may be an indispensable task for the coupling of adjacent components. Moreover, the implementation of the proposed method in such a context would be significantly useful for the optimization and validation of design approaches in offshore WTs [50].

4.2. Case B: wind turbine tower section

This example is focused on the response prediction of the tower section shown in Fig. 6(a), with the aim of further illustrating the effectiveness and applicability of the method in components experiencing rigid body modes. The considered sec-

$\gamma_{b,1}$ $\gamma_{b,2}$ $\gamma_{b,3}$ $\gamma_{b,4}$ $\gamma_{b,5}$ $\gamma_{b,6}$ $\gamma_{b,7}$ $\gamma_{b,8}$
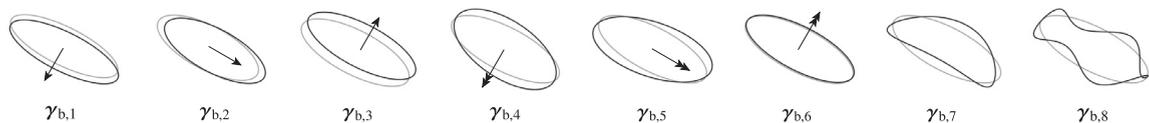
Fig. 3. The first eight components of the reduction basis for the tower-top interface; gray and black lines denote the undeformed and deformed interface respectively.

Table 2
Diagonal entries of the process noise $\mathbf{Q}^{pp}$ related to the driving inputs of the tower substructure.

Method	Basis size			Generalized interface forces					
	n_ϕ / n_f	n_γ	$\tilde{\mathbf{g}}_{b,1}$	$\tilde{\mathbf{g}}_{b,2}$	$\tilde{\mathbf{g}}_{b,3}$	$\tilde{\mathbf{g}}_{b,4}$	$\tilde{\mathbf{g}}_{b,5}$	$\tilde{\mathbf{g}}_{b,6}$
Fixed-interface	2	6	2.0e4	5.0e3	1.0e-3	8.0e3	1.0e4	1.0e1
Free-interface	2	6	1.0e5	5.0e3	1.0e-3	1.0e4	2.0e4	4.0e1
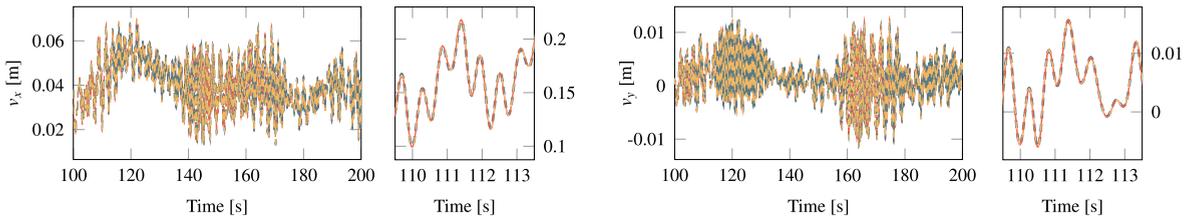
Fig. 4. Actual (black) versus estimated fore-aft and side-to-side displacement response at the validation point; estimates using the fixed-interface model are represented by red line; free-interface estimates are denoted by continuous orange line. (For interpretation of the references to colour in this figure legend, the reader is referred to the web version of this article.)
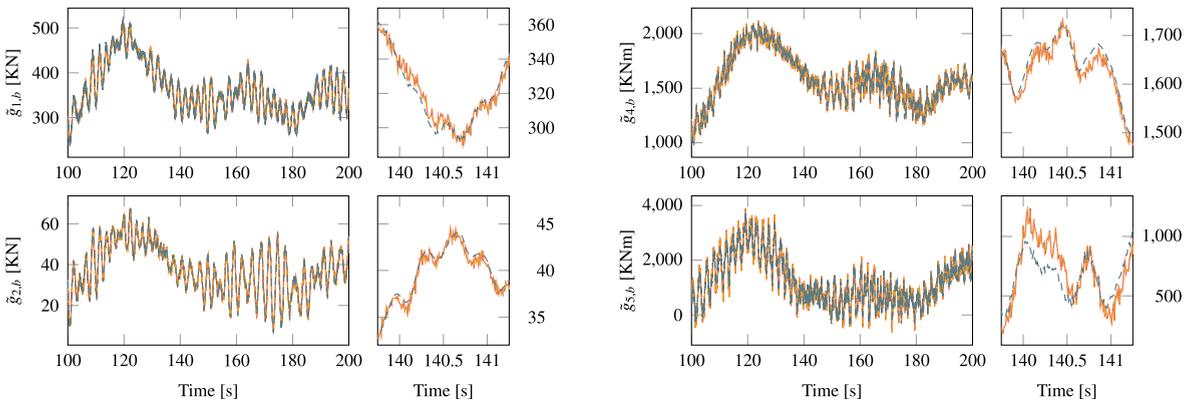
Fig. 5. Equilibrium conditions at the tower-top interface - Actual (black) versus estimated fore-aft and side-to-side interface forces; estimates using the fixed-interface model are represented by red line; free-interface estimates are denoted by continuous orange line. (For interpretation of the references to colour in this figure legend, the reader is referred to the web version of this article.)
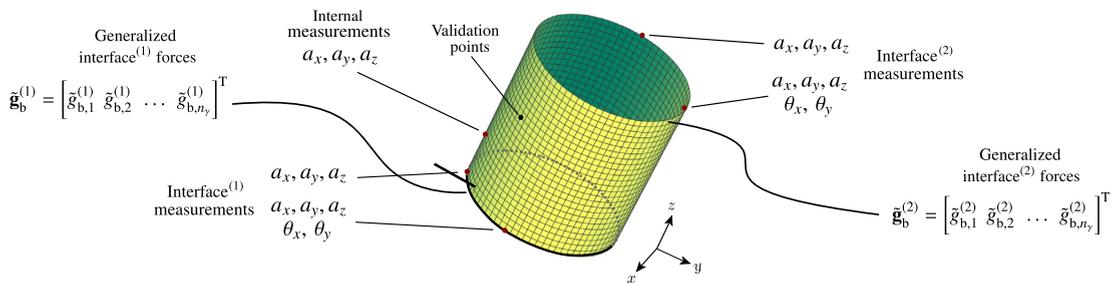
Fig. 6. The tower-section substructure model and the measured interface and internal response quantities.

tion is 5 m long and constitutes the upper substructure of the tower examined in the previous case study, with the bottom diameter of 4.00 m located at 82.6 m from the ground level and the top diameter, equal to 3.87 m, being the interface with rotor-nacelle assembly. It should be noted that the usefulness of such a monitoring approach might not be initially evident, but it is significantly relevant in the context of vibration assessment and fatigue monitoring of critical weld seams and/or flanges, whereby tower sections are connected, or even for substructure model updating and hybrid testing applications.

To this end, the vibration response obtained from the full WT model at the measurement locations shown in Fig. 6 are fused with the substructure model through the Bayesian filter in order to recursively estimate the entire dynamic state and the unmeasured generalized interface forces, which are assumed to exclusively drive the tower-section dynamics. Again, the substructure is modeled using both Craig-Bampton and Rubin methods, with the aim of highlighting the different reduction ingredients and most importantly the performance and specifics of each model in terms of response prediction and observability conditions. Based on the discussion of the previous section and given that the tower is well characterized by the beam theory assumptions, the interface reduction of the substructure is again carried out assuming rigidified cross-sections, whose response is described by the six rigid body modes, as shown in Fig. 3.

With the global tower response being dominated by the first two vibration modes in fore-aft and side-to-side directions [47], the bending-induced displacement field of the tower section can be accurately approximated by retaining a limited number of fixed- or free-interface modes in each direction for the Craig-Bampton or Rubin method, respectively. This may be conceptually evidenced through Fig. 7(b) and (c), which depicts the first two vibration modes of each method. When these are coupled with the six rigid body movements of each interface through the constraint and residual attachment modes, the substructure response spanned by the first two global tower modes can be approximated without the need of retaining components higher than the first two. It should be noted though that even in that case, the contribution of higher-order modes might be also statically significant [51], due to the coupling of generalized coordinates $\mathbf{q}_i, \mathbf{q}_b$ and $\mathbf{q}_f, \mathbf{q}_b$.

To investigate the significance of this coupling and determine the required order of the reduction basis for the internal degrees of freedom, the ROM of the substructure is initially constructed using only one component in each direction from each basis $\boldsymbol{\Phi}$ and $\boldsymbol{\Xi}$, for fixed- and free-interface methods, respectively. Upon discarding the components related to purely axial vibration, the basis vectors required in order to accurately capture the bending behavior in x and y directions are determined using Algorithm 1, with the displacement response at the validation point being used as reference measurement. The initial model for each method comprises only the first internal basis vector and the relative tolerance for the assessment of each candidate model is set to 1%. The results obtained for the bending components in y direction using the two methods are illustrated in Fig. 8, where circular marks indicate the vectors appended in the basis and "x" marks denote the ones being rejected. As evidenced through Fig. 8, an accurate prediction can be obtained using two and three basis vectors for the fixed- and free-interface schemes, respectively. Such a difference may be attributed to the local behavior contained in the fixed-interface modes, as opposed to the free ones, which may be indicatively highlighted by comparing ϕ_2 with ξ_2 in Fig. 7. With similar results obtained for bending behavior in x direction, the ROM constructed with Craig-Bampton method comprises two bending components in each direction x and y, one torsional and six interface modes for each one of the interfaces, resulting in a system of 17 basis vectors. On the other hand, the Rubin-based ROM comprises 3 bending components in each direction, one torsional, twelve interface and another six rigid body modes, leading to a total of 25 generalized degrees of freedom.

In order for the two reduced-order substructure systems to be observable, none of the terms $\mathbf{S}_d\mathbf{T}$ and $\mathbf{S}_a\mathbf{T}$ must contain any zero columns. Moreover, due to the fact that the tower section model experiences rigid-body motions, stability of the system cannot be ensured using only strain and acceleration measurements. Additional displacement information at the boundaries should be utilized in order to ensure stability of the inversion and further enable the identification of rigid-body motion. Although the latter might not be of interest in the context of structural dynamics, it is inevitably contained in acceleration and inclination measurements and therefore has to be accommodated by the model. In this example, displacements in longitudinal direction due to bending are obtained through tilt measurements, while the ones in transverse directions are extracted from accelerations. The latter is not directly measurable in practice, but can be numerically calculated through the integration of acceleration signals [52,53]. Accordingly, the displacements in longitudinal direction can be also obtained through integration and in that case tilt measurements would be redundant leading thus to the minimum number of sensors, namely six acceleration channels in each interface and three in the internal domain.

For the estimation step, the filter of each model is initialized with $\mathbf{z}_0 = \mathbf{0}$ and $\mathbf{P}_0 = 10^3 \cdot \mathbf{I}$, where $\mathbf{I} \in \mathbb{R}^{2n}$ is the identity matrix. The measurement noise covariance matrix $\mathbf{R}$ is adjusted according to the added sensor noise, which amounts to 3% of the signals standard deviation, and the process noise covariance associated with the generalized displacements and velocities is chosen equal to $\mathbf{Q}^{xx} = 10^{-7} \cdot \mathbf{I}$. The process noise $\mathbf{Q}^{pp}$ related to the system inputs is assumed to have a diagonal

(a) Fixed-interface modes   (b) Free-interface modes
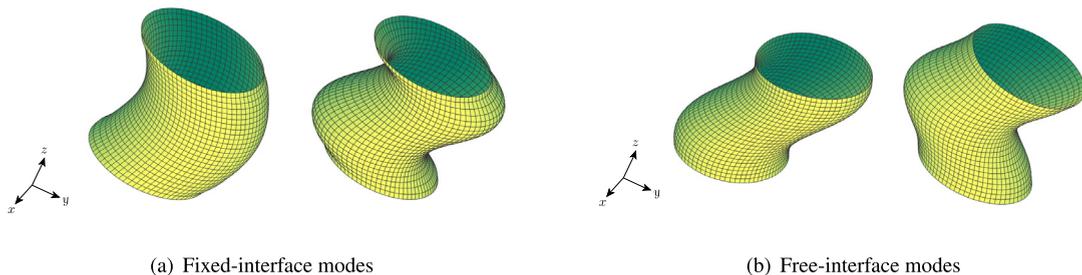
Fig. 7. The first two reduction components for bending in y direction using (a) fixed- and (b) free-interface substructure schemes.
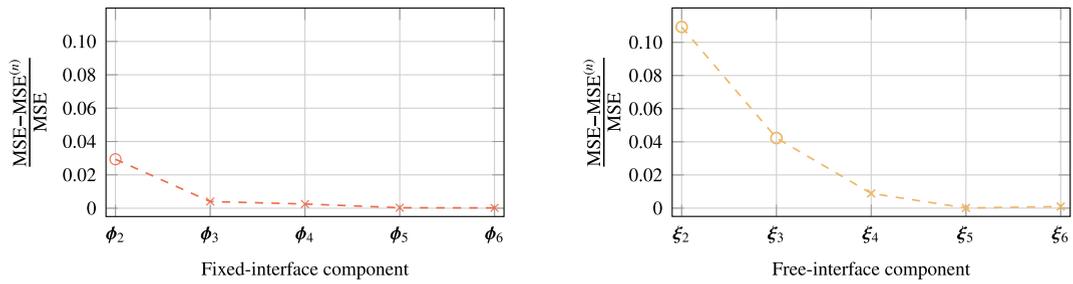
Fig. 8. Selection of basis vectors for fixed- (left) and free-interface methods (right).

structure and is tuned on the basis of the L-curve [53]. The latter is essentially an n_p-dimensional curve, whose optimal point is obtained upon separation of the problem into n_p L-curves, one for each entry of $\mathbf{Q}^{pp}$. As such, the optimal point is sequentially obtained for all curves and the process is repeated until convergence of all entries, with the final values documented in Table 3. The results obtained in terms of interface force estimates in fore-aft direction are plotted in Fig. 9 against the actual values, which are obtained upon projecting the interface forces obtained from the forward simulation of the entire WT model on the interface reduction basis $\mathbf{\Gamma}_b^T$. The estimates of $\tilde{g}_{b,1}$, which essentially represents the thrust force are seen to be slightly biased which is mainly owed to the fact that this forcing term is strongly associated with the integration-based displacement measurements. On the other hand, the corresponding fore-aft bending moment estimates, which are strongly related to the inclination measurements, are very accurately tracked using either model. A similar picture is observed in Fig. 10, where the estimated displacement response in the unmeasured location, shown in Fig. 6, is also well predicted with both models.

4.3. Wind turbine blade

The last case-study is focused on the NREL 5-MW WT blade, whose structural details are also documented in [44]. To highlight the capabilities and limitations of the proposed approach, the implementation of this case-study is based on a three-dimensional FE model of the blade, which is developed independently of the rest of the system. The model is constructed using (linear) 4-noded and six-degree-of-freedom thin shell elements, which are employed with a reduced-integration scheme and hourglass control [54], so as to attenuate numerical artifacts. In the absence of information pertaining to the properties and orientation of each individual layer of the glass-fiber material, the characterization of the composite material is carried out by an inverse process, whereby the six engineering constants of an effective orthotropic material are calibrated in order to achieve a satisfactory agreement between the first FE modal properties and those occurring from the equivalent beam properties reported in [44].

In order to achieve an as close to reality as possible representation of the vibration response, the dynamic behavior of the blade is obtained by means of an aeroelastic analysis, which is based on the Blade Element Momentum (BEM) [55] theory. Due to the fact that the one-dimensional loads (drag, lift and aerodynamic moment) obtained from the latter are not directly applicable to three-dimensional FE models, a hybrid scheme combining BEM with airfoil pressure distributions, derived from XFOIL, is devised. Namely, the blade is, similarly to the conventional BEM approach, discretized into a number of blade elements on which the angle of attack is obtained using BEM theory. Thereafter, the loads are not extracted in the form of drag and lift terms but instead, the angle of attack is used to compute the pressure distribution over the central section of each blade element using Xfoil. Lastly, the pressure at intermediate mesh points is computed by interpolation.

The motivation behind this application stems mainly from the fact that blades are currently among the least condition-monitored WT components, due to their size, the uncertainty related to loading conditions as well as due to the lack of understanding of the effects induced by local defects. With the instrumentation of existing blades being feasible only at the vicinity of the root, several practical limitations are imposed in the full-scale vibration monitoring of such structures. In this sense, the proposed substructure-based approach is well suited for monitoring the transition region between the root and the zone of airfoil profile, which is the most fatigue- and damage-critical location [56,57] of blades. Moreover, it enables the implementation of a more sophisticated control scheme that would not only aim at regulating the generator speed but

Table 3
Diagonal entries of the process noise $\mathbf{Q}^{pp}$ related to the driving inputs of the tower section.

Method	Basis size		Interface[1]						Interface[2]					
	n_ϕ/n_f	n_γ	$\tilde{g}_{b,1}^{(1)}$	$\tilde{g}_{b,2}^{(1)}$	$\tilde{g}_{b,3}^{(1)}$	$\tilde{g}_{b,4}^{(1)}$	$\tilde{g}_{b,5}^{(1)}$	$\tilde{g}_{b,6}^{(1)}$	$\tilde{g}_{b,1}^{(2)}$	$\tilde{g}_{b,2}^{(2)}$	$\tilde{g}_{b,3}^{(2)}$	$\tilde{g}_{b,4}^{(2)}$	$\tilde{g}_{b,5}^{(2)}$	$\tilde{g}_{b,6}^{(2)}$
Fixed	5	12	3.5e4	1.0e3	1.0e−3	2.0e3	1.0e4	5.0e1	3.5e4	1.0e3	1.0e−3	2.0e3	1.0e4	5.0e1
Free	7	12	5.0e4	1.0e3	1.0e−5	5.0e4	1.0e4	1.0e2	5.0e4	1.0e3	1.0e−5	5.0e4	1.0e4	1.0e2
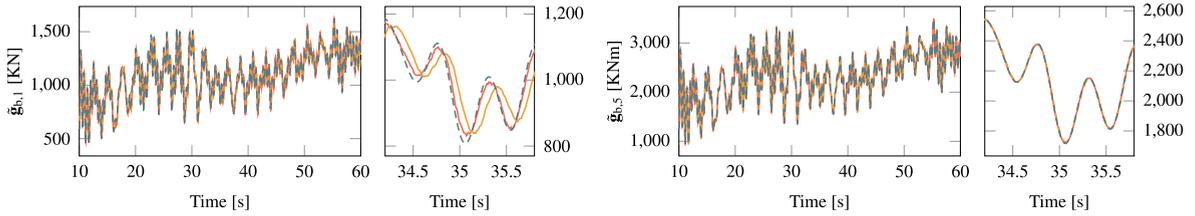
Fig. 9. Actual (black dashed) versus estimated tower-top interface force (left) and moment (right) in fore-aft direction; estimates using the fixed-interface model are represented by red line; free-interface estimates are denoted by continuous orange line. (For interpretation of the references to colour in this figure legend, the reader is referred to the web version of this article.)
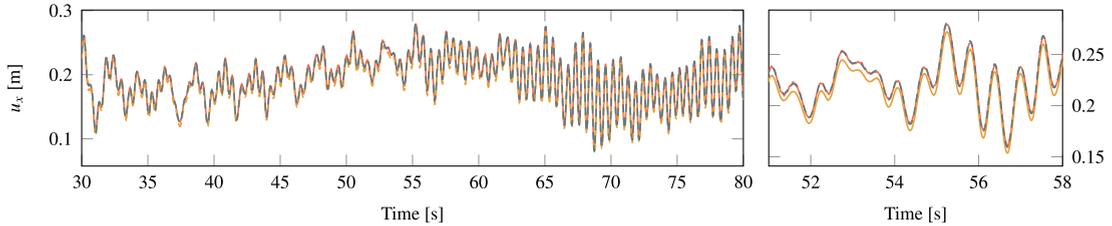
Fig. 10. Actual (black dashed) versus estimated displacement response at the validation point; estimates using the fixed-interface model are represented by red line; free-interface estimates are denoted by continuous orange line.

also at minimizing the fatigue-induced damage in these critical regions. Lastly, the modeling of complex dynamics occurring at the tip of the blade [58], which are characterized by large uncertainties associated with both the aerodynamic damping and the vortex-dominated behavior, are thereby avoided and their effect on the substructure of interest may be reflected through the estimated interface forces.

In contrast with the tower, whose cross-section kinematics are in compliance with the rigid interface reduction, blades are characterized by more complex behavior at the cross-section level, which includes both in-plane and out-of-plane warping effects [59,60]. Although such information is already contained in a full three-dimensional FE model of the blade, it has to be additionally injected at the substructure level, through the interface modeling, in order to accurately capture the non-modeled dynamics. To initially illustrate the dominance of warping at the cross-section deformation, the entire blade is simulated under realistic operational conditions, as described above, and a snapshot of the deformed airfoil located at the substructure interface is illustrated in Fig. 13(a). It can be seen that apart from rigid body movements, assumed by beam theory, the interface experiences an out-of-plane deformation which need be taken into account using higher-order interface modes. As such, the interface reduction is performed using 7 components, including the six rigid-body translations and rotations as well as one warping component, as shown in Fig. 13(b).

In applications where the system dynamics are driven by concentrated loads with known spatial distribution, the input can be estimated using the expressions of Table 1 for the transformation matrix $\bar{\mathbf{T}}$. However, as the number of excitation forces increases, the estimation may become quickly ill-conditioned, as is the case in aerodynamic and hydrodynamic problems, where the load is exerted as time-varying distributed pressure. In this sense, and in order to further ensure a unique relation between input and state, the input at the level of the blade can be estimated only in the space of generalized coordinates. As such, the input to be estimated, which is also assumed to be driving the substructure dynamics, comprises the generalized interface forces as well as the fixed- and free-interface modal forces for each method, respectively. These terms
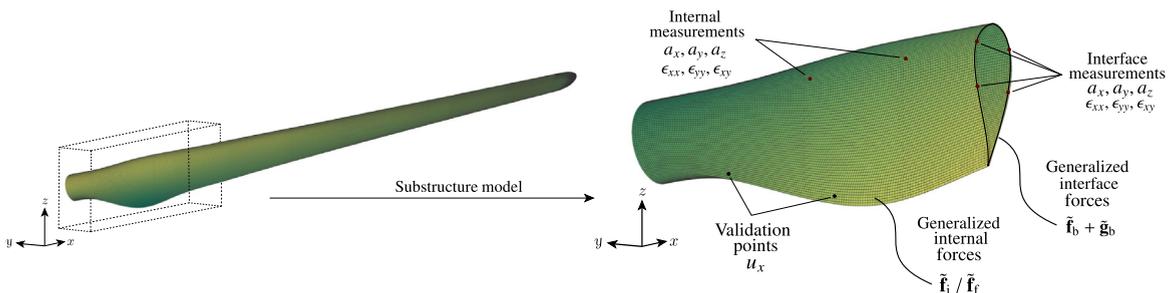
Fig. 11. The WT-blade used for forward simulations (left) and the substructure set-up (right) used for response and input identification.

Table 4
Estimated generalized forces under unknown input spatial distribution using the fixed- and free-interface methods.

Method	Forces	Description
Fixed-interface	$\tilde{\mathbf{f}}_i = \mathbf{\Phi}_i^T \mathbf{S}_{p_i} \mathbf{p}_i$	Generalized fixed-interface forces
	$\tilde{\mathbf{h}}_b = \tilde{\mathbf{f}}_b + \tilde{\mathbf{g}}_b = \mathbf{\Gamma}_b^T(\mathbf{\Psi}_b^T \mathbf{S}_{p_i} \mathbf{p}_i + \mathbf{g}_b)$	Generalized interface forces
Free-interface	$\tilde{\mathbf{f}}_f = \left(\mathbf{\Xi}_i^T - \mathbf{\Xi}_b^T \mathbf{K}_{bb}^{(\Lambda)} \mathbf{\Lambda}_i^T\right) \mathbf{S}_{p_i} \mathbf{p}_i$	Generalized free-interface forces
	$\tilde{\mathbf{h}}_b = \tilde{\mathbf{f}}_b + \tilde{\mathbf{g}}_b = \mathbf{\Gamma}_b^T\left(\mathbf{K}_{bb}^{(\Lambda)} \mathbf{\Lambda}_i^T \mathbf{S}_{p_i} \mathbf{p}_i + \mathbf{g}_b\right)$	Generalized interface forces
	$\tilde{\mathbf{f}}_r = \left(\mathbf{R}_i^T - \mathbf{R}_b^T \mathbf{K}_{bb}^{(\Lambda)} \mathbf{\Lambda}_i^T\right) \mathbf{S}_{p_i} \mathbf{p}_i$	Rigid-body forces

are documented in Table 4, where it is further shown that the contribution of $\mathbf{p}_i$ and $\mathbf{g}_b$ is practically inseparable due to the fact that $\mathbf{p}_i$ is exerted as distributed load however, the total nodal interface forces can be still retrieved through Eq. (39), by replacing $\tilde{\mathbf{g}}_b$ with $\tilde{\mathbf{f}}_b + \tilde{\mathbf{g}}_b$, to yield $\mathbf{f}_b + \mathbf{g}_b = \left(\mathbf{\Gamma}_b^T\right)^\dagger \left(\tilde{\mathbf{f}}_b + \tilde{\mathbf{g}}_b\right)$.

Similarly to the tower dynamics, the blade response is typically dominated by the first few vibration modes [61]. Therefore, the displacement field of the blade substructure can be well approximated by retaining the first few internal $\mathbf{q}_i$ and free $\mathbf{q}_f$ vibration modes. The importance of each one of those candidate modes is again assessed using Algorithm 1, resulting thus to 3 and 5 significant components for each method, respectively. As briefly mentioned in Section 3, the number of these modes is a determinant factor for the maximum number of generalized forces $\mathbf{f}_i$ and $\mathbf{f}_f$ to be estimated, which is on the other side limited by the number of sensors located at the internal degrees of freedom. In this sense, the fixed-interface model consists in total of ten basis vectors and the substructure dynamics are driven by seven interface and three internal generalized forces. On the other hand, the free-interface model is constructed using twelve free modes and the corresponding dynamics are assumed to be driven by the same interface forces and another five free-mode generalized loads. In the example presented in this paper, only a single point of operational parameters of the WT is considered, which allows for the reduction basis to be statically defined. However, it should be noted that the dynamics of blades are strongly dependent on the operational conditions of the WT and therefore the reduction basis components might need be adapted accordingly.

The estimation algorithm is initialized for both models with a zero-mean state $\mathbf{z}_0$ and a corresponding error covariance estimate $\mathbf{P}_0 = 10^5 \cdot \mathbf{I}$, where $\mathbf{I} \in \mathbb{R}^{2n}$ denotes the identity matrix. The values of the measurement noise covariance matrix $\mathbf{R}$ are specified in accordance with the added sensor noise, while the process noise covariance matrix related to the non-augmented states, i.e., the displacement and velocity terms, are for both models adjusted to $\mathbf{Q}^{xx} = 10^{-8} \cdot \mathbf{I}$. The major difference in the performance of the two estimators, which is assessed in terms of the accuracy in tracking the unmeasured state, input and response at validation points, is owed to the noise term $\mathbf{Q}^{pp}$, which is related to the augmented part of the state, i.e., the driving inputs. As such, $\mathbf{Q}^{pp}$ is assumed to be a diagonal matrix, whose values are tuned by means of the L-curve, upon following the same process described in Section 4.2. This results in the values reported in Table 5 for the diagonal entries related to the fixed- and free-mode generalized forces as well as for the corresponding values of the interface forces.

Table 5
Diagonal entries of the process noise $\mathbf{Q}^{pp}$ related to the driving inputs of the blade substructure

Method	Basis size	Generalized fixed/free-interface forces			Generalized interface forces						
	n_γ	$\bar{\mathbf{f}}_{i,1}/\bar{\mathbf{f}}_{f,1}$	$\bar{\mathbf{f}}_{i,2}/\bar{\mathbf{f}}_{f,2}$	$\bar{\mathbf{f}}_{i,3}/\bar{\mathbf{f}}_{f,3}$	$\bar{\mathbf{h}}_{b,1}$	$\bar{\mathbf{h}}_{b,2}$	$\bar{\mathbf{h}}_{b,3}$	$\bar{\mathbf{h}}_{b,4}$	$\bar{\mathbf{h}}_{b,5}$	$\bar{\mathbf{h}}_{b,6}$	$\bar{\mathbf{h}}_{b,7}$
Fixed-interface	3	7	5.0e1	8.5e−1	7.0e−1	1.0e4	1.0e4	1.0e4	1.0e4	1.0e4	1.0e4	1.0e4
Free-interface	5	7	1.2e−1	0.5e−1	0.4e−1	1.0e4	1.0e4	1.0e4	1.0e4	1.0e6	1.0e6	1.0e7

(a) Fixed-interface components   (b) Free-interface components
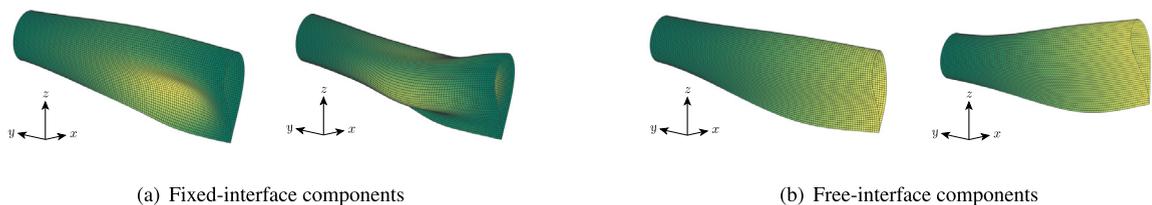
Fig. 12. The first two fixed- and free-interface components of the blade substructure.
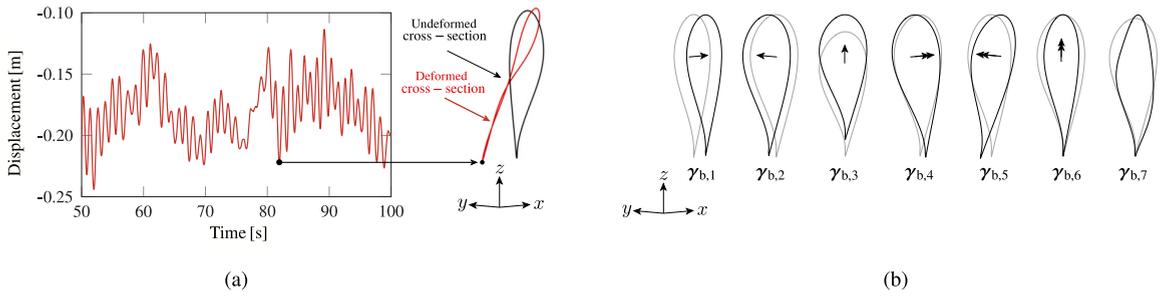
Fig. 13. Deformed shape of the substructure interface (a) and the corresponding reduction basis components (b); gray and black lines denote the undeformed and deformed interface respectively.

The estimates of the first fixed- and free-interface mode are plotted on the left-hand side of Fig. 14 against their actual values. It should be noted that the forward problem for the generation of simulation measurements is performed on the entire WT blade and therefore the actual values of such quantities, i.e., $\mathbf{q}_{i,1}$ and $\mathbf{q}_{f,1}$ are not readily available. However, these are extracted by projecting the aerodynamic loads and interface forces of the full WT blade model into the reduction basis $\bar{\mathbf{T}}^T$ and subsequently solving the forward problem for each substructure model. As evidenced from Fig. 14, a sufficiently accurate estimate is obtained for both $\mathbf{q}_{i,1}$ and $\mathbf{q}_{f,1}$, while it is further seen that the vibration mode ξ_1 associated with the latter is evidently more significant than ϕ_1 for the representation of the substructure displacement field. Such a conclusion may be also intuitively drawn from Fig. 12 which illustrates the local nature of the first two fixed-interface modes against their free-interface counterparts. The right-hand side of Fig. 14 depicts the estimated edgewise and flapwise bending moments at the interface respectively, with the Rubin-based estimates showing an offset with respect to the actual values, which may be attributed to the biased estimates of the corresponding generalized forces, as will be further discussed in the following paragraphs.

The estimated generalized interface forces are presented in Fig. 15, along with the actual values, which are again obtained by projecting the load components $\mathbf{p}_i$ and $\mathbf{g}_b$ into the reduction basis $\bar{\mathbf{T}}^T$. It is seen that the three plotted components $\tilde{\mathbf{h}}_{b,4}$, $\tilde{\mathbf{h}}_{b,6}$ and $\tilde{\mathbf{h}}_{b,7}$, which essentially represent the edgewise bending moment, flapwise bending moment and warping force respectively, are accurately and almost identically predicted using both models. The estimates of force terms $\tilde{\mathbf{f}}_i$ and $\tilde{\mathbf{f}}_f$, which are related to the aerodynamic loads exerted on the internal degrees of freedom of the substructure, are depicted in Fig. 16. Due to the fact that these loads are projected on the reduced space through different basis vectors for each method, they are not directly comparable. As such, the left-hand side column of Fig. 16 depicts the fixed-mode loads while the free-mode counterparts are presented on the right-hand side column. Except for the first two components of the free-method, which are proven to be significantly sensitive to the corresponding noise terms due to their major contribution in the total response, all inputs are accurately identified.

Lastly, the predicted flapwise response in the two validation points located at the transition zone, as shown in Fig. 11, is plotted in Fig. 17. A small offset can be observed on the estimated displacements obtained with the fixed-interface model, despite the accurate prediction of both states and loads. On the other hand, the offset noticed in the interface force estimates obtained with the free-interface model appears to be compensated by the opposite bias in the corresponding generalized
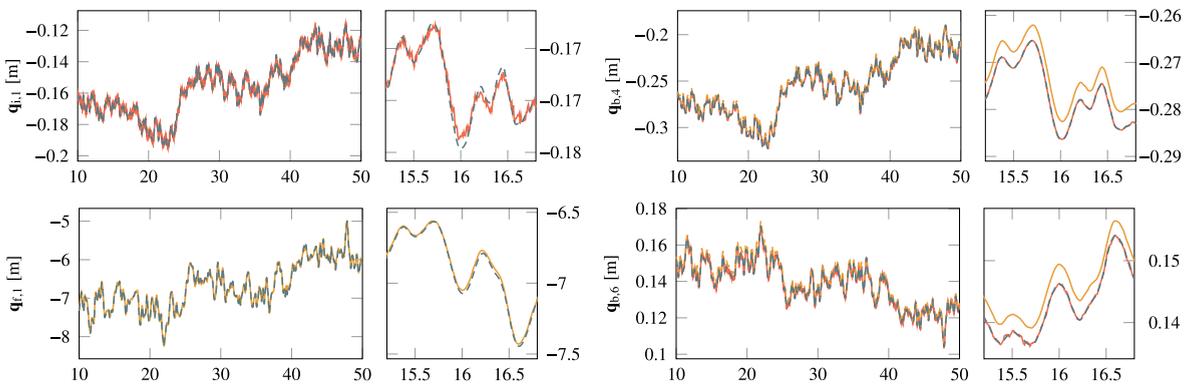
Fig. 14. Actual (black dashed) versus estimated internal (left) and interface (right) state; estimates using the fixed-interface model are represented by red line; free-interface estimates are denoted by continuous orange line. (For interpretation of the references to colour in this figure legend, the reader is referred to the web version of this article.)
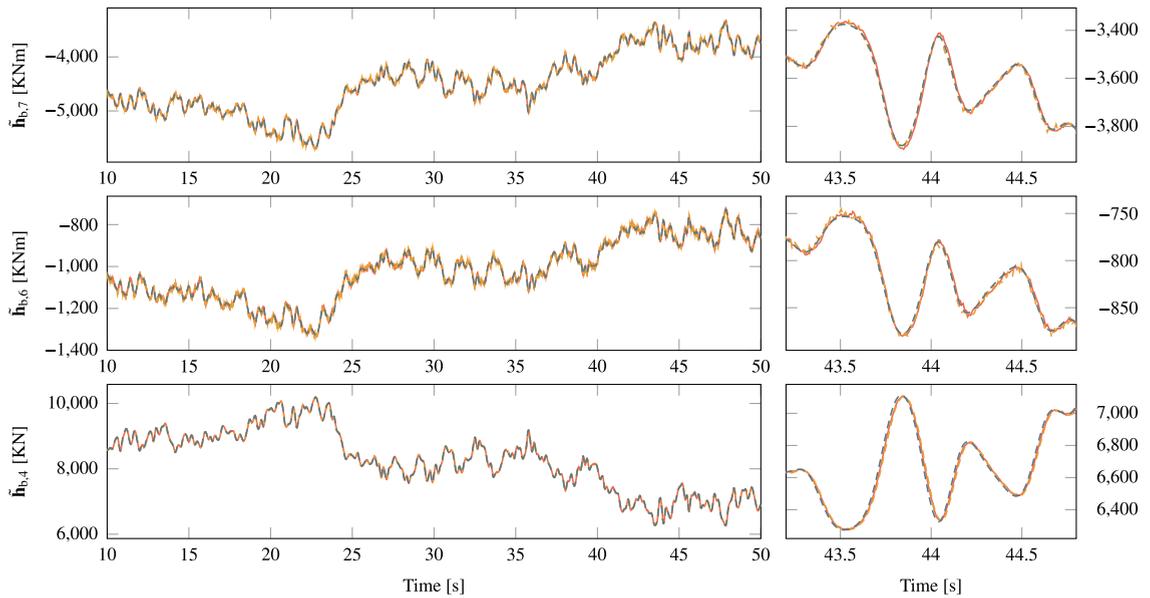
Fig. 15. Actual (black dashed) versus estimated edgewise moment (bottom), flapwise moment (middle) and warping force (top) at the interface; estimates using the fixed-interface model are represented by red line; free-interface estimates are denoted by continuous orange line. (For interpretation of the references to colour in this figure legend, the reader is referred to the web version of this article.)

internal loads, resulting thus in a highly accurate estimate of the unmeasured quantities. It should be noted that the two methods are generally not equivalent for the same number of basis vectors [62], which is also evidenced from the fact that a different number of components is required, using the proposed selection algorithm, in order to succeed a comparable performance in terms of the estimated unknown quantities with the two models. Moreover, the presented results indicate that the superiority of one method against the other is not easily deducible, but has to be assessed in the context of a specific target application.
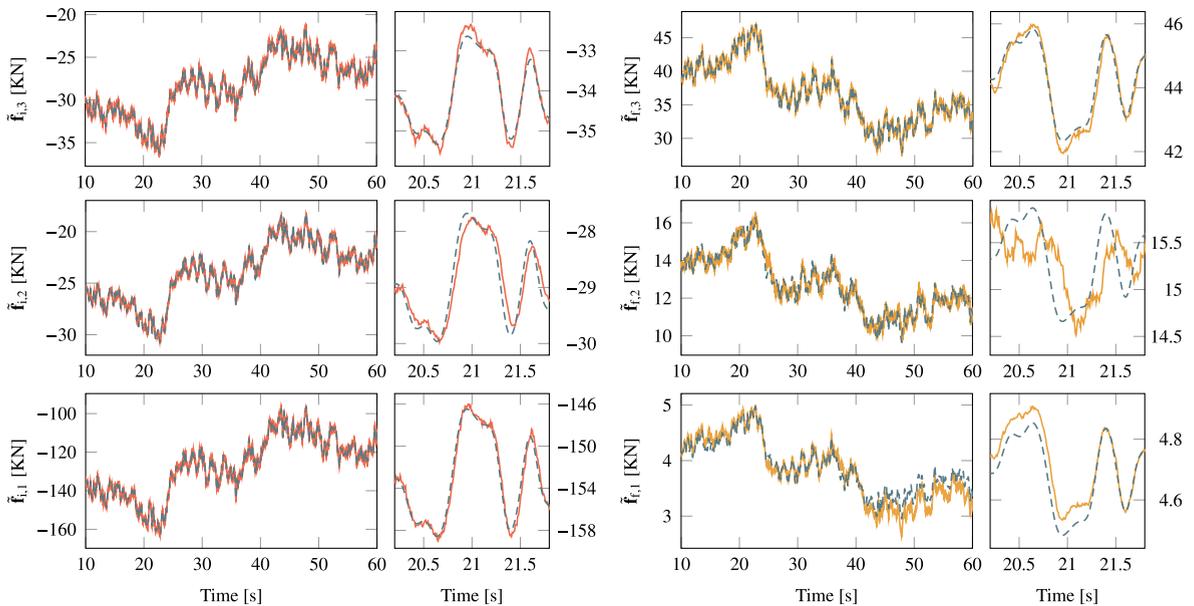
Fig. 16. Actual (black dashed) versus estimated fixed- (left) and free-interface (right) generalized forces; estimates using the fixed-interface model are represented by red line; free-interface estimates are denoted by continuous orange line. (For interpretation of the references to colour in this figure legend, the reader is referred to the web version of this article.)
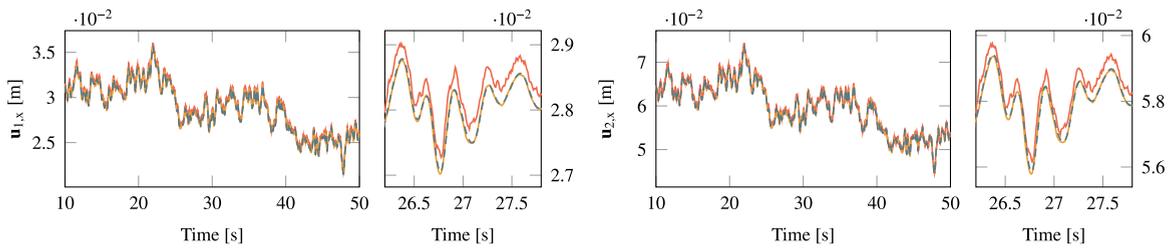
Fig. 17. Actual (black dashed) versus estimated flapwise displacement in the validation points; estimates using the fixed-interface model are represented by red line; free-interface estimates are denoted by continuous orange line. (For interpretation of the references to colour in this figure legend, the reader is referred to the web version of this article.)

5. Conclusions

This study established the theoretical formulation and presented the practical implementation of a general framework for component-based response identification of dynamic systems using output-only sensing information, by coupling substructuring techniques and output-only Bayesian filters. The proposed framework is based on the premise that the dynamics of a system subdomain are driven by (i) the externally applied loads and (ii) the interface forces, with the latter reflecting the unaccounted for system components. As such, the problem of substructure response prediction based on a limited number of vibration measurements is tailored to an input-state estimation context, which is recursively solved using a Bayesian filter. The methodology is formulated on the basis of both fixed- and free-interface substructure approaches namely, the Craig-Bampton and Rubin methods.

The proposed framework was tested and assessed via three simulated examples on WT systems, whereby it was shown that the generalized system state, the dynamic response at unmeasured locations and the unknown driving forces can be accurately estimated, on the basis of a limited number of output measurements. Within this context, the interface reduction constitutes a determinant step for the representation of unaccounted for system dynamics and despite the fact that the two examined modeling methods are not equivalent for the same number of basis vectors, it was demonstrated that comparable results may be delivered by properly selecting the reduced-order space components. The applicability of the method is further extended to systems with unknown or distributed input locations, such as WT blades, by performing the estimation on the space of generalized input coordinates.

Regarding the performance of the two substructuring methodologies, it can be observed that for most of the cases a model of lower order is generated by the fixed-interface approach, leading thus to a model of higher computational efficiency, which also favors real-time and online performance. To a certain extent, this is owed to the fact that rigid body modes are not contained in the free-interface modes but are included as additional basis components, which need be further calculated and create an additional offline cost for the Rubin-based model. However, the major advantage of the latter consists in the fact that the free-interface modes comprise a more natural, rather than artificial, system feature which can be experimentally extracted from a free-free vibration test, providing thus the possibility of substituting the underlying numerical model with one that is experimentally determined.

Since the congruence of the underlying model with the actual system dynamics is a critical factor for the performance of recursive Bayesian estimators, the proposed framework may well serve as means of reducing the model uncertainty, by focusing only on the domain or component of interest. An indicative example along these lines was presented for a WT tower, where the entire state can be retrieved without the need for modeling the intricate rotor dynamics. Lastly, the method can be further implemented for component-based model updating, hybrid testing applications or utilized as a guideline for monitoring campaigns targeted to specific components rather than the entire system.

Declaration of Competing Interest

The authors declare that they have no known competing financial interests or personal relationships that could have appeared to influence the work reported in this paper.

Acknowledgements

References

[1] L.J. Nordström, T.P. Nordberg, A time delay method to solve non-collocated input estimation problems, Mech. Syst. Signal Process. 18 (2004) 1469–1483.
[2] D. Bernal, A. Ussia, Sequential deconvolution input reconstruction, Mech. Syst. Signal Process. 50–51 (2015) 41–55.
[3] D. Bernal, Non-recursive sequential input deconvolution, Mech. Syst. Signal Process. 82 (2017) 296–306.
[4] F. Naets, J. Croes, W. Desmet, An online coupled state/input/parameter estimation approach for structural dynamics, Comput. Methods Appl. Mech. Eng. 283 (2015) 1167–1188.
[5] F. Naets, J. Cuadrado, W. Desmet, Stable force identification in structural dynamics using Kalman filtering and dummy-measurements, Mech. Syst. Signal Process. 50–51 (2015) 235–248.
[6] S. Gillijns, B. De Moor, Unbiased minimum-variance input and state estimation for linear discrete-time systems, Automatica 43 (2007) 934–937.
[7] S. Gillijns, B. De Moor, Unbiased minimum-variance input and state estimation for linear discrete-time systems with direct feedthrough, Automatica 43 (2007) 934–937.
[8] E. Lourens, E. Reynders, G. De Roeck, G. Degrande, G. Lombaert, An augmented Kalman filter for force identification in structural dynamics, Mech. Syst. Signal Process. 27 (2012) 446–460.
[9] S. Eftekhar Azam, E. Chatzi, C. Papadimitriou, A dual Kalman filter approach for state estimation via output-only acceleration measurements, Mech. Syst. Signal Process. 60 (2015) 866–886.
[10] V.K. Dertimanis, E.N. Chatzi, S. Eftekhar Azam, C. Papadimitriou, Input-state-parameter estimation of structural systems from limited output information, Mech. Syst. Signal Process. 126 (2019) 711–746.
[11] S.E. Azam, E. Chatzi, C. Papadimitriou, A. Smyth, Experimental validation of the Kalman-type filters for online and real-time state and input estimation, J. Vib. Control 23 (2015) 1–26.
[12] J.C. Doyle, K. Glover, P.P. Khargonekar, B.A. Francis, State-space solutions to Standard H2 and Hinfinity Control Problems, IEEE Trans. Autom. Conrol 34 (1989) 831–847.
[13] E.N. Chatzi, A.W. Smyth, The unscented Kalman filter and particle filter methods for nonlinear structural system identification with non-collocated heterogeneous sensing, Struct. Control Health Monitor. 16 (2009) 99–123.
[14] E.N. Chatzi, A.W. Smyth, Nonlinear system identification: particle-based methods, Encycl. Earthq. Eng. (2014).
[15] J.N. Yang, S. Pan, H. Huang, An adaptive extended Kalman filter for structural damage identification, Struct. Control Health Monitor. 14 (2007) 497–521.
[16] S.S. Bisht, M.P. Singh, An adaptive unscented Kalman filter for tracking sudden stiffness changes, Mech. Syst. Signal Process. 49 (2014) 181–195.
[17] C. Papadimitriou, C.-P. Fritzen, P. Kraemer, E. Ntotsios, Fatigue predictions in entire body of metallic structures from a limited number of vibration sensors using Kalman filtering, Struct. Control Health Monitor. 18 (2011) 554–573.
[18] V. Dertimanis, E. Chatzi, S. Azam, C. Papadimitriou, Output-only fatigue prediction of uncertain steel structures, in: 8th European Workshop on Structural Health Monitoring, EWSHM 2016, Bilbao, Spain, 2016..
[19] D. Giagopoulos, A. Arailopoulos, V. Dertimanis, C. Papadimitriou, E. Chatzi, K. Grompanopoulos, Computational framework for online estimation of fatigue damage using vibration measurements from a limited number of sensors, Procedia Eng. 199 (2017) 1906–1911.
[20] N. Noppe, K. Tatsis, E.N. Chatzi, C. Devriendt, W. Weijtjens, Fatigue stress estimation of offshore wind turbine using a Kalman filter in combination with accelerometers, in: International Conference on Noise and Vibration Engineering (ISMA 2018), 2018.
[21] H.A. Jensen, E. Millas, D. Kusanovic, C. Papadimitriou, Model-reduction techniques for Bayesian finite element model updating using dynamic response data, Comput. Methods Appl. Mech. Eng. 279 (2014) 301–324.
[22] K. Tatsis, V. Dertimanis, I. Abdallah, E. Chatzi, A substructure approach for fatigue assessment on wind turbine support structures using output-only measurements, Procedia Eng. 199 (2017) 1044–1049.
[23] L. Wu, P. Tiso, K. Tatsis, E. Chatzi, F. van Keulen, A modal derivatives enhanced Rubin substructuring method for geometrically nonlinear multibody systems, Multibody Syst. Dyn. (2018).
[24] K. Tatsis, L. Wu, P. Tiso, E. Chatzi, State estimation of geometrically non-linear systems using reduced-order models, in: Proceedings of the 6th International Symposium on Life-Cycle Civil Engineering Ghent, Belgium, 2018.
[25] K.V. Yuen, K. Huang, Identifiability-enhanced Bayesian frequency-domain substructure identification, Comput. Aided Civil Infrastruct. Eng. 33 (2018) 800–812.
[26] E. Lourens, D.J.M. Fallais, Full-field response monitoring in structural systems driven by a set of identified equivalent forces, Mech. Syst. Signal Process. 114 (2019) 106–119.
[27] C. Papadimitriou, D.C. Papadioti, Component mode synthesis techniques for finite element model updating, Comput. Struct. 126 (2013) 15–28.
[28] R.L. Mayes, M.R. Ross, Advancements in hybrid dynamic models combining experimental and finite element substructures, Mech. Syst. Signal Process. 31 (2012) 56–66.
[29] S. Puerto Tchemodanova, K. Tatsis, V. Dertimanis, E. Chatzi, M. Sanayei, Remaining fatigue life prediction of a roller coaster subjected to multiaxial nonproportional loading using limited measured strain locations, in: Structures Congress 2019, Florida, USA, 2019, pp. 112–121..
[30] R.J. Guyan, Reduction of stiffness and mass matrices, AIAA J. 3 (1965), 380–380.
[31] B. Irons, Structural eigenvalue problems – elimination of unwanted variables, AIAA J. 3 (1965) 961–962.
[32] R.R.J. Craig, M.C.C. Bampton, Coupling of substructures for dynamic analyses, AIAA J. 6 (1968) 1313–1319.
[33] H. MacNeal, Richard, A hybrid method of component mode synthesis, Comput. Struct. 1 (1971) 581–601.
[34] S. Rubin, Improved component-mode representation for structural dynamic analysis, AIAA J. 13 (1975) 995–1006.
[35] D.J. Rixen, A dual Craig-Bampton method for dynamic substructuring, J. Comput. Appl. Math. 168 (2004) 383–391.
[36] R.R.J. Craig, A.J. Kurdila, Fundamentals of Structural Dynamics, John Wiley & Sons (2006), https://doi.org/10.1115/1.801667.ch3.
[37] M. Geradin, D.J. Rixen, Mechanical Vibrations Theory and Application to Structural Dynamics, Wiley, 2015.
[38] M.P. Castanier, Y.-C. Tan, C. Pierre, Characteristic constraint modes for component mode synthesis, AIAA J. 39 (2001) 1182–1187.
[39] K. Maes, E. Lourens, K. Van Nimmen, E. Reynders, G. De Roeck, G. Lombaert, Design of sensor networks for instantaneous inversion of modally reduced order models in structural dynamics, Mech. Syst. Signal Process. 52–53 (2015) 628–644.
[40] B. Peherstorfer, K. Willcox, Dynamic data-driven reduced-order models, Comput. Methods Appl. Mech. Eng. 291 (2015) 21–41.
[41] K. Tatsis, E. Lourens, A comparison of two Kalman-type filters for robust extrapolation of offshore wind turbine support structure response, in: Fifth International Symposium on Life-Cycle Civil Engineering (IALCCE 2016), Proceedings of the Fifth International Symposium on Life-Cycle Civil Engineering (IALCCE 2016), Delft, The Netherlands, 2016, pp. 209–216..
[42] T.J. Rogers, K. Worden, G. Manson, U.T. Tygesen, E.J. Cross, A Bayesian filtering approach to operational modal analysis with recovery of forcing signals, in: Proceedings of ISMA 2018 – International Conference on Noise and Vibration Engineering and USD 2018 – International Conference on Uncertainty in Structural Dynamics, 2018, pp. 5181–5194.
[43] R. Nayek, S. Chakraborty, S. Narasimhan, A Gaussian process latent force model for joint input-state estimation in linear structural systems, Mech. Syst. Signal Process. 128 (2019) 497–530.
[44] B.J. Jonkman, TurbSim User's Guide, Technical Report, National Renewable Energy Laboratory, Battelle, CO, USA, 2009.
[45] E. Hau, Wind Turbines, Fundamentals, Technologies, Application, Economics, Springer, 2006.
[46] M. Feyzollahzadeh, M.J. Mahmoodi, S.M. Yadavar-Nikravesh, J. Jamali, Wind load response of offshore wind turbine towers with fixed monopile platform, J. Wind Eng. Ind. Aerodyn. 158 (2016) 122–138.
[47] C. Devriendt, F. Magalhães, M. El Kafafy, G. De Sitter, Á. Cunha, P. Guillaume, Long-term dynamic monitoring of an offshore wind turbine, Conference Proceedings of the Society for Experimental Mechanics Series, 39, 2013..

[48] D.C. Kammer, M.J. Triller, Selection of component modes for craig-bampton substructure representations, J. Vib. Acoust. Trans. ASME 118 (1996) 264–270.
[49] P.J. Moylan, Stable inversion of linear systems, IEEE Trans. Autom. Control (1977) 74–78.
[50] M. Hall, A. Goupee, J. Jonkman, Development of performance specifications for hybrid modeling of floating wind turbines in wave basin tests, J. Ocean Eng. Mar. Energy 4 (2018).
[51] H.A. Jensen, A. Muñoz, C. Papadimitriou, C. Vergara, An enhanced substructure coupling technique for dynamic re-analyses: application to simulation-based problems, Comput. Methods Appl. Mech. Eng. 307 (2016) 215–234.
[52] A. Smyth, M. Wu, Multi-rate Kalman filtering for the data fusion of displacement and acceleration response measurements in dynamic system monitoring, Mech. Syst. Signal Process. 21 (2007) 706–723.
[53] H.B. Gilbert, O. Celik, M.K. O'Malley, Long-term double integration of acceleration for position sensing and frequency domain system identification, IEEE/ASME International Conference on Advanced Intelligent Mechatronics, AIM, 2010, pp. 453–458.
[54] Hibbit, Karlsson, Sorensen, ABAQUS: theory manual, 1992.
[55] M.O.L. Hansen, Aerodynamics of Wind Turbines, Taylor & Francis Ltd (2015), https://doi.org/10.1017/CBO9781107415324.004.
[56] J.C. Marín, A. Barroso, F. París, J. Cañas, Study of fatigue damage in wind turbine blades, Eng. Failure Anal. 16 (2009) 656–668.
[57] H.G. Lee, M.G. Kang, J. Park, Fatigue failure of a composite wind turbine blade at its root end, Compos. Struct. 133 (2015) 878–885.
[58] J. Johansen, N.N. Sørensen, Numerical Investigation of Three Wind Turbine Blade Tips, Technical Report, Forskningscenter Risoe, Risoe, 2002..
[59] D. Chortis, Structural Analysis of Composite Wind Turbine Blades, Springer, 2013.
[60] S. Han, O.A. Bauchau, On the nonlinear extension-twist coupling of beams, Eur. J. Mech., A/Solids 72 (2018) 111–119.
[61] M.H. Hansen, Aeroelastic instability problems for wind turbines, Wind Energy 10 (2007) 551–577.
[62] D.C. Kammer, M. Baker, Comparison of the Craig-Bampton and residual flexibility methods of substructure representation, J. Aircraft 24 (1987) 262–267.